Computational modelling of peri-personal space representation in schizophrenia spectrum disorders

Renato Paredes Venero

Master of Science

Cognitive Science

School of Informatics

University of Edinburgh

2019

Abstract

The encoding of the space close to the body, named peri-personal space (PPS), is thought to be relevant to explain the abnormal experiences of the self observed in schizophrenia (SCZ). However, current conceptual accounts do not agree with recent empirical evidence that directly observed the PPS in SCZ and high schizotypy (H-SPQ). More precisely, it is unclear why SCZ patients and H-SPQ individuals present a narrower PPS and why the boundaries of the PPS are sharply defined in patients. In this context, we hypothesise that the unusual PPS representation observed in SCZ is caused by an imbalance of excitation and inhibition (E/I) in recurrent synapses of unisensory neurons and an impairment of bottom-up and top-down synapses between unisensory and multisensory neurons.

These hypothesis were tested computationally by modelling the influence of SCZ in a neural network originally designed to encode PPS representations of healthy individuals. This was done by including two parameters in the model to simulate the effects of E/I imbalance (β) and synaptic density decrease (ρ) in the network mechanics. We computed simulations to explore the effects of both impairments in the PPS representation generated by the network and fitted the model to experimental data to test our hypotheses.

Results showed that disinhibition of sensory neurons cause the small PPS observed in SCZ ($\beta = 4.49$) and H-SPQ ($\beta = 4.30$), whereas a decrease of bottom-up and top-down synaptic density causes the sharp definition of the PPS observed in SCZ (a decrease of 24.35 %). Moreover, based on the exploration of the model mechanics, we predicted that disinhibition also causes poor tactile discrimination and personal space enlargement in SCZ.

Based on these results, we proposed a novel conceptual model of PPS representation in the SCZ spectrum compatible with current empirical evidence of self-aberrations, personal space, tactile discrimination and symptoms observed in patients. This model relates the aforementioned behavioural observations and symptoms computationally by describing the effects disinhibition in cortical areas involved in the spatial encoding of sensory stimulation.

Acknowledgements

I would like to thank my supervisor, Dr. Peggy Series, whose expertise was invaluable in motivating this project. Her sharp and accurate feedback throughout the dissertation period was fundamental for the culmination of this work.

I would also like to thank Dr. Francesca Ferri for sharing the data of the empirical study modelled in this project and encouraging the development of this research.

I want to acknowledge my friends, who were of great support during my studies. I would like to specially thank Ms. Suganya Sundaravadivelu for her invaluable presence throughout this year.

In addition, I would like to thank my parents for making possible my sole presence in this program and always believing in me.

Finally, I want to thank Mataji Shaktiananda for her divine teachings and the inspiration to investigate the Self.

Table of Contents

Chapter 1

Introduction

Schizophrenia (SCZ) is considered a major neuropsychiatric disorder due to the amount of disabilities it produces. One core characteristic of this disorder is the abnormal subjective experience of the self, clinically denominated as self-disturbances. This involves alterations in the stream of consciousness, bodily self-experience and self-demarcation, which lead to the subjective perception of an unclear distinction between the self and the external world [1, 2].

Recent literature proposes that the neural mechanisms responsible for the encoding of the peri-personal space (PPS) (i.e. the space near the body) play an important role in the abnormal perceptions of the self [3]. Although this view has been explored conceptually [3] and empirically [4], little is known about the underlying mechanisms behind the PPS encoding in SCZ. In this context, this research is aimed to implement a computational model able to give account of PPS encoding in the SCZ spectrum and contribute to the understanding of self-disturbances.

1.1 Background

1.1.1 Computational modelling of SCZ

Early computational models of SCZ were focused on particular mechanisms that were thought to give rise to specific symptoms of the disease. For example, anatomical impairments in the form of disruption of white matter tracts during brain development were proposed to be the cause of hallucinations and thought disorder symptoms [5, 6]. Similarly, impairments in corollary discharge (i.e. the mechanism responsible for disregarding self-initiated actions) were thought to cause failures to distinguish the

origin of self-generated actions and thoughts from those that were externally generated [7, 8]. More recently, failures in dopamine signalling produced by NMDA receptors impairment resulting in an imbalance of excitation and inhibition (E/I) are thought to be the origin of positive symptoms such as hallucinations and delusions [9, 10, 11].

Currently, a relevant tendency on the field is the effort to create a broader theoretical framework compatible with previous models and capable of accounting for the multiple symptoms that characterise the disease [12, 13, 14]. Researchers committed with this endeavour propose that the broad symptomatology of SCZ could be explained in terms of Bayesian inference and a predictive coding account of the brain. This account aims to integrate perception, action and cognition as a multilevel process of top-down inferences and bottom-up error corrections that occur in the brain (see [15] for a comprehensive review). More precisely, this view proposes the brain as a predictive machinery that is constantly making inferences ("guessing") about the external, propioceptive and interoceptive inputs it receives. By doing so, it is constantly adjusting and updating its predictions whenever discrepancies between a predicted sensory outcome and a sensory event occur (i.e. prediction errors). At the neural level, such hierarchical process would be possible due to predictive signals sent through NMDA receptors and prediction errors signals sent via glutamatergic AMPA receptors [16, 17].

From a predictive coding perspective, SCZ is understood as an impairment in the precision attributed to prior sensory beliefs or sensory data which produces inferences mainly dominated by sensory data [14]. This is thought to be produced by hypofunctioning of cortical NMDA receptors and GABA neurons along with elevated activity of striatal dopamine D_2 receptors, in agreement with the E/I imbalance hypothesis evidence [11]. According to this framework, such signalling dysfunction leads to a strong weighting of prediction errors, which in turn causes abnormal learning that needs to be explained by delusional beliefs [18]. Moreover, this predictive coding account of SCZ may also provide explanations in terms of failures in Bayesian inference for hallucinations [19, 20, 21, 22], as well as for thought insertions and experiences of external control [23, 24]. Furthermore, evidence of anatomical and structural connectivity abnormalities found in patients [25, 26] could be understood as a consequence of the above mentioned abnormal functional integration (i.e. failures in signalling across different levels of the hierarchy) that produces changes in morphometry or tractography [13].

1.1.2 Peri-personal space (PPS)

The brain encodes the space that surrounds the body to interact with the environment. This space representations are split into regions according to their distance from the body: PPS (the space reachable by hand) and extrapersonal space (the space that cannot be reached by hand) [27] (see Figure 1.1). This view is supported by evidence of fronto-parietal neurons responding stronger to visual and auditory stimulation that occurs near the body in macaques [28, 29] and humans [30, 31, 32, 33, 34, 35] (see [36] for an extensive review). From an evolutionary perspective, these neurons are thought to encode the PPS to respond faster to stimuli near the body as a mechanism against threats from the environment [37].

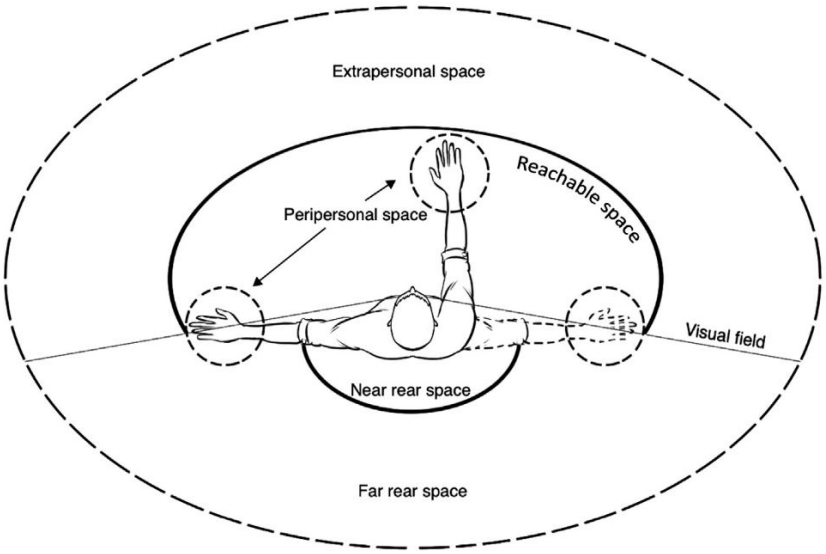

Figure 1.1: Diagram of the space around the body. The image shows the classification of the spaces around the body according to their distance from the body. Image taken from [27]

The receptive field (RF) properties of the PPS neurons (i.e. size, response preferences and spatial frames of reference) have been studied behaviourally in a well established experimental paradigm [38, 39]. This experiment involved delivering approaching and receding auditory or visual stimuli and measuring the reaction times (RT) of participants to tactile stimulation (see Section 2.1 for more details). Research within this paradigm reveal that the PPS can be extended after synchronous tactile and auditory stimulation in the extrapersonal space [40]. Plus, the size of the PPS is different across the body and is encoded holding the trunk as a common reference frame [39].

Evidence from bodily self-consciousness experiments [1] (e.g. Enfacement Illusion, Body-Swap Illusion and Full Body Illusion) have led to the hypothesis that PPS representation is relevant to bodily self-consciousness processes in the brain [41, 42]. More precisely, it has been proposed that PPS representation is crucial in the causal inference process of bodily self-consciousness because it couples body-related information and surrounding exteroceptive signals [43]. Overall, the PPS could be better understood as the "space of the self" [44].

1.1.3 Computational modelling of PPS representation

A mechanistic description of the PPS dynamics was modelled employing a neural network designed to mimic fronto-parietal multisensory networks that encode the PPS representation [45]. In short, the model considers two upstream unisensory areas connected with a downstream multisensory area that holds multisensory representations of the PPS (see Section 2.2 for more details). Originally the model was conceived to reproduce the visuo-tactile representation of the PPS around both hands, but later adaptations of the model have been developed to encode audio-tactile representations of the PPS around the hand [40] and the trunk [46].

This model is able to simulate RT responses of healthy participants in the aforementioned audio-tactile experimental paradigm [38]. More precisely, it reproduces that faster responses are obtained when auditory stimuli are administered in the space close to the hand due to a selective response of the multisensory neuron for stimuli in the PPS [40]. In addition, the model is able to reproduce changes in the PPS boundaries either by synchronous bimodal sensory stimulation [40] or the velocity of the incoming stimuli [46] as observed in empirical studies. These findings suggest that such model is a suitable framework to study PPS representations and support the view that it can be employed for evaluating treatments and diseases [45].

1.1.4 PPS representation in SCZ

An unusual PPS representation is thought to be behind self-disturbances in SCZ. Particularly, it has been proposed that schizophrenic patients hold a weaker or more variable PPS representation [3]. This view is based on the observation that schizophrenic patients are more prone to experience bodily self-aberrations such as the Rubber Hand

[1] These experiments were built to manipulate feelings of body ownership in participants as a result of controlled multimodal stimulation.

Illusion (RHI) [2] [47] and the Pinocchio Illusion (PI) [3][48].

As a consequence, a working model was proposed suggesting that space representations in SCZ are characterised by a shallow gradient dividing the PPS and the extrapersonal space. More precisely, a shallower demarcation of the PPS is thought be an indicator of reduced self demarcation (i.e. confusion of boundaries between self and others and permeability of self-world boundaries) [3]. This view has been partially supported by evidence relating a shallower PPS boundary and reports of unusual experiences [4] after audiovisual sensory deprivation [50].

Recently, this working model was empirically tested in the aforementioned audio-tactile paradigm [38]. The experiment revealed that schizophrenic patients (N = 18) and high-schizotypy (H-SPQ) individuals (N = 18) present a narrower PPS compared to healthy controls (HC) (N = 18) (Cohen's d = .86) and low-schizotypy (L-SPQ) individuals (N = 18) (Cohen's d = .86) respectively [4]. However, contrary to conceptual predictions, it was found that schizophrenic patients present sharper PPS boundaries (i.e. steeper gradients dividing the PPS and the extrapersonal space) compared to controls (Cohen's d = .81). In addition, it was found that PPS extension was negatively correlated with negative symptoms [5] and positive/negative symptoms ratio in SCZ. Although the study holds some limitations (e.g. small sample size, the PPS representation was not measured in all directions), it was the first to directly evaluate conceptual conjectures regarding the PPS representation in SCZ spectrum disorders and provides an initial framework to model such representation computationally.

Furthermore, a relevant body of literature related to this phenomena is the study of personal space (i.e. the distance at which one person feels comfortable in the presence of another individual) in schizophrenic patients. Particularly, such research has consistently revealed that personal space is enlarged in patients and that such enlargement is correlated with negative symptoms of SCZ [52, 53, 54, 55, 56, 57, 58]. At the neurobiological level, the personal space is thought to be encoded by a specific fronto-parietal network comprised by the ventral premotor cortex (PMv) and the dorsal intraparietal sulcus (DIPS) [59], which has been found to be impaired in schizophrenic patients.

[2]The RHI is an experimental paradigm designed to generate in participants the feeling that a rubber hand is their own, as a result of synchronous or asynchronous stimulation of the fake hand and their real hand (which is not visible to participants).

[3]The PI is an experimental paradigm designed to generate in participants the sensation that their nose is growing in response to tactile-proprioceptive stimulation .

[4]Unusual experiences is a subscale of the Oxford-Liverpool Inventory of Feelings and Experiences [49] that measures positive symptoms of psychosis.

[5]Negative symptoms refer to deficits in the initiation and maintenance of activities, emotional experience and communication [51]

Specifically, it was found that in patients the DIPS region was hyper-responsive to social stimuli and that such hyper-activity was related to both the size of the personal space and the presence of negative symptoms [58].

1.2 Problem statement

Although there is qualitative, experimental and neurocognitive evidence of self-disturbances as an early marker of SCZ [2, 3], little is known about the underlying neural computations that originate this trait. From a predictive coding account, it has been proposed that an impairment in sensory attenuation due to failures in Bayesian inferences computed in the brain may be behind self-disturbances such as thought insertions and external control [23, 24]. However, this account has not been able to integrate the experimental and theoretical advances in the study of human PPS representation [42], its suggested relationship with bodily self-consciousness [41, 44] and its potential implications in self-disturbances [3].

Furthermore, the specific neural basis and mechanics of the observed PPS representation in schizophrenic patients and individuals with schizotypal traits is unknown. There has not been an in depth examination of the disagreement between the working model of PPS representation in SCZ [3] and the aforementioned experimental evidence [4]. Particularly, a comprehensive explanation of why schizophrenic patients and individuals with schizotypal traits present a narrower PPS is lacking. Similarly, there is not a theoretical understanding of why PPS boundaries are sharply defined in schizophrenic patients when the current working model [3], indirectly supported by recent empirical evidence [50], predicted a shallower definition of such boundaries.

Moreover, it is unclear why the size of the PPS and the personal space seem to be inversely related in schizophrenic patients. This observation is particularly odd given that both spaces are encoded by fronto-parietal networks [59, 36] and are thought to be part of a defensive architecture dedicated to regulate the space close to the body against potential threats [60]. Similarly, alterations in both spaces have been found to be correlated with negative symptoms of SCZ [58, 4], which suggests that both alterations are related to a same category of impairments observed in the disease.

In sum, it is elusive what is the shared neural impairment in SCZ that gives rise to alterations in the PPS, personal space, negative symptoms and deficits in social cognition (see [51] for a review of the neural basis of social cognition deficits and negative symptoms). Similarly, it is unclear what common impaired mechanism is

behind a small and sharply defined PPS representation and the propensity of patients to manifest bodily self-aberrations and positive symptoms (e.g. hallucinations, delusions, etc.) associated with self-disturbances.

1.3 Objectives and Hypothesis

This research is aimed to implement a computational model that can account for PPS representation in SCZ and schizotypy [4] and is compatible with state of the start computational modelling of psychosis [13, 14]. For this purpose, a recurrent neural network model of PPS [45, 40] will be adapted to reproduce PPS changes observed in SCZ (i.e. size reduction and boundaries sharpening) in a simulated audio-tactile behavioural task. The simulated results will be compared against experimental data of schizophrenic patients and individuals with high schizotypal traits [4]. The adapted models will then be explored to generate predictions regarding personal space resizing and bodily self-aberrations.

We hypothesise that a narrower PPS representation in SCZ spectrum disorders is a result of an E/I imbalance in recurrent synapses among unisensory neurons, in agreement with neurobiological evidence [11] and the predictive coding account of psychosis [13, 14]. Moreover, we expect that PPS boundaries sharpening in SCZ may be explained in terms of an impairment of bottom-up and top-down synapses between unisensory and multisensory neurons, in line with anatomical observations [25, 26]. Finally, we conjecture that both E/I modulation and synaptic impairments are related to alterations in the personal space and bodily self-aberrations observed in patients.

Chapter 2

Methods

2.1 Experimental task

The network model is ought to be examined in a simulated task that mimics the experiment undertaken with schizophrenic patients and H-SPQ individuals in the aforementioned study [4]. This experiment consisted of presenting approaching and receding sounds to participants at different distance points combined with a tactile stimulation. At every trial, participants were required to respond to the tactile stimulation by pressing a button with their left index finger.

The illusion of different distances was generated by manipulating the intensity of the sound and the delay relative to the sound onset at which the tactile stimulation was administered. The changing intensity of the sound generated the subjective feeling of a sound approaching or receding. Hence, the delay from the sound onset allowed to provide tactile stimulation when the sound is located at a specific distance from the participant. For example, for looming sounds the larger the delay, the closer is the sound perceived by the participant.

For this purpose, two speakers were located in front of the participants at two different positions: one at 100cm and the other next to their right hand, as shown in Figure 2.1. The auditory stimuli were samples of pink noise of 3000 ms duration with flat (constant 62.5 dB) or increasing (exponentially rising from 55 to 70 dB) intensity levels. The tactile stimulus was a constant voltage (between 60 and 90 mA, according to the sensitivity threshold of each participant) of 100 µs provided by a pair of electrodes located in the right index finger. Only five different delays (300 ms, 800 ms, 1500 ms, 2200 ms and 2700 ms) were considered for the experiment, as in the original experimental protocol [38].

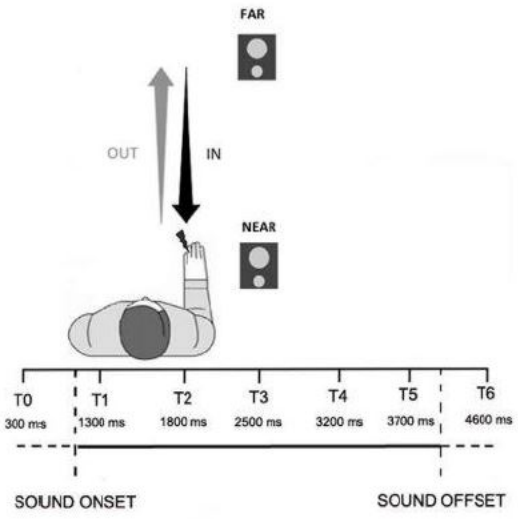

Figure 2.1: PPS audio-tactile experimental paradigm. The figure shows the experimental setup composed by two speakers in front of the participant and an electrode in his hand. The arrows indicate the idea of sounds moving towards or away from the participant with tactile stimulation administered at different delays from the sound onset. Image taken from [38]

The RT of participants to tactile stimulation was registered in 18 trials to examine differences in responses due to the location of the sound at the moment of the tactile stimulation. This paradigm is built on the observation that faster responses occur when stimuli is administered in the space near the body due to the activity of the PPS neurons [37, 38].

The average RT obtained from the looming sounds were fitted to a sigmoid function. This function is intended to depict the PPS representation and its parameters represent the features of such representation. Hence, the central point (CP) of the curve is interpreted as the extend of the PPS, whereas the slope is understood as the steepness of the PPS boundary. In the empirical study [4], it was found that SCZ patients presented higher CPs (i.e. a smaller PPS) and steeper slopes than HC, whereas H-SPQ individuals displayed only higher CPs in comparison with L-SPQ individuals (see Figure 2.2).

2.2 Neural network model of PPS representation

A theoretical neural network model built to mimic the mechanisms of audio-tactile PPS representation around the right hand will be employed [40]. This model is an adap-

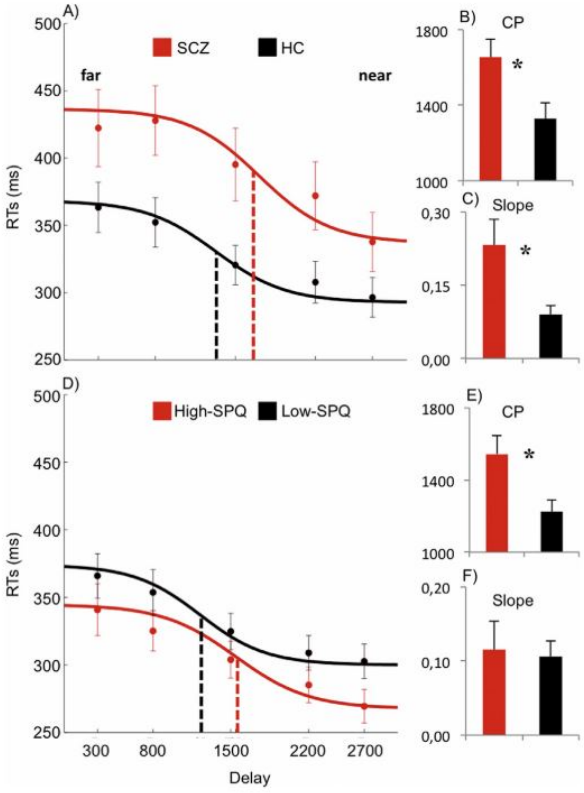

Figure 2.2: Results of the empirical study with SCZ patients and H-SPQ individuals. Panels A,B and C reveal that in SCZ the PPS boundary (i.e. CP) is located at a smaller distance and registers a steeper slope compared to controls (HC). In contrast, panels D,E and F show that the PPS boundary of H-SPQ individuals is located at a smaller distance compared to L-SPQ individuals. Image taken from [4].

tation of an earlier network designed for visuo-tactile interaction in the space around both hands [61, 45] to deal with audio-tactile interaction in only one hand. Although a newer version of the network has been developed recently [46], the aforementioned model was selected because it was designed to be tested under the same experimental paradigm [38] employed in the empirical study with SCZ patients and H-SPQ individuals [4].

Extensive details regarding its implementation can be found in the supplementary material of the original publication [40]. An overview of its implementation and functioning is presented in this section. The numerical values of the parameters to be presented can be found in Appendix A.1.

2.2.1 Network architecture

The model is composed of two recurrently connected unisensory areas (auditory and tactile) interacting with one multisensory area (see Figure 2.3). Each neuron in both unisensory areas has its own receptive field (RF) defined in hand-centred in coordinates (along the horizontal and vertical axis) and responds to stimulation received by an external input with specific spatial coordinates in relation to the hand. In the following, x_i^s and y_j^s will denote the centre of the RF of a given neuron at position ij of the unisensory area s, where s can be either t (tactile) or a (auditory).

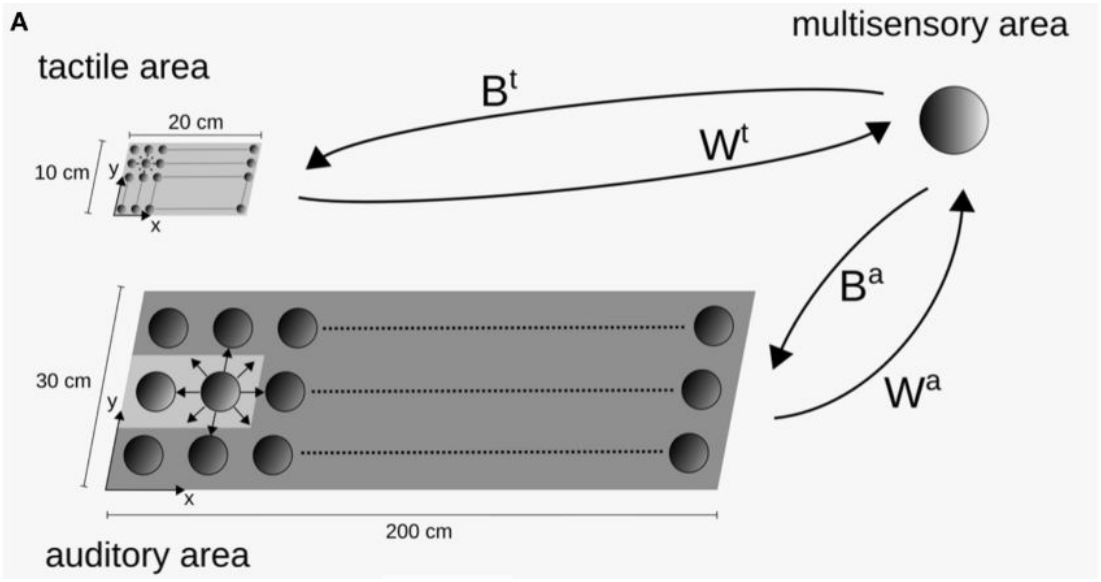

Figure 2.3: Model of PPS audio-tactile representation. The network is composed of two unisensory areas connected with a multisensory area. Each unisensory area is arranged according to a specific topological organisation to encode the external space. Image taken from [40].

The tactile area is composed of 800 neurons (disposed in a $M^t = 40$ x $N^t = 20$ grid) that encode a skin portion of 20 cm x 10 cm corresponding to the left hand of an individual. This area may roughly represent high-order somatosensory areas in the parietal lobe [62, 63]. The tactile RF centres coordinates are defined by Equation 2.1.

$$x_i^t = i \cdot 0.5cm (i = 1,2,..,M^t) \qquad y_j^t = j \cdot 0.5cm (j = 1,2,..,N^t) \tag{2.1}$$

Similarly, the auditory area is composed of 60 neurons (disposed in a $M^a = 20$ x $N^a = 3$ grid) that cover an auditory space of 200 cm x 30 cm on and around the hand. Here it must be noted that the auditory area is composed of fewer neurons that encode

larger spaces to mimic the lower spatial resolution of the auditory system. Hence, this auditory area roughly resembles high-order neural structures of the auditory pathway that encode the spatial location of the sound source [29]. The auditory RF centres coordinates are defined by Equation 2.2.

$$x_i^a = i \cdot 10 - 5cm (i = 1,2,..,M^a) \qquad y_j^a = j \cdot 10 - 15cm (j = 1,2,..,N^a) \tag{2.2}$$

Finally, the multisensory area is composed of a single neuron that is connected to all neurons in both auditory and tactile areas. This composition reveals that the RF of the multisensory neuron has a wider spatial extension compared to individual unisensory neurons and that several unisensory neurons converge to a single multisensory neuron [61]. This design is congruent with the observation that only few multisensory neurons are capable of encoding the entire space of the hand [64, 65, 66, 67].

2.2.2 Network synapses

Each neuron of the unisensory areas is recurrently connected to all neurons in the area to which it belongs. These synaptic connections are symmetrical and are arranged in a "Mexican hat" pattern, which promotes excitation of neurons that are closer and fosters inhibition in neurons that are further. In this setup, an external stimulus activates a limited number of unisensory neurons and avoids the propagation of excitation in the unisensory area. The specific weights assigned to the synapses are obtained as the difference between two Gaussian functions (one excitatory and one inhibitory), according to equation 2.3.

$$L^s_{ij,hk} = \begin{cases} L^s_{ex} \cdot exp\left(-\frac{(D^s_x)^2+\left(D^s_y\right)^2}{2\cdot\left(\sigma^s_{ex}\right)^2}\right) - L^s_{in} \cdot exp\left(-\frac{(D^s_x)^2+\left(D^s_y\right)^2}{2\cdot\left(\sigma^s_{in}\right)^2}\right), & ij \neq hk \\ 0, & ij = hk \end{cases} \tag{2.3}$$
$$s = t, a$$

$L^s_{ij,hk}$ denotes the weight of the synapse from the pre-synaptic neuron at position hk to post-synaptic neuron at position ij. D^s_x and D^s_y indicate the distances between the pre-synaptic neuron and the post-synaptic neurons along the horizontal and vertical axis of the unisensory area. The excitatory Gaussian function is defined by parameters L^s_{ex} and σ^s_{ex}, whereas the inhibitory is defined by L^s_{in} and σ^s_{in}. A null term (i.e. zero) is included in equation 2.3 to avoid auto-excitation. The weights of the recurrent synapses of both auditory and tactile areas are presented in Figure 2.4.

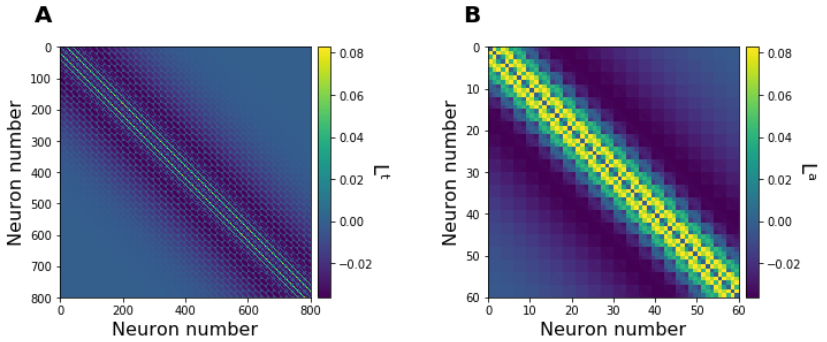

Figure 2.4: Network recurrent connections. The colours displayed in the images represent the strength of the synapses. The neurons are indexed according to their position in the grid. The numbering starts from the neuron located in the fist row and column and progresses column-wise.

The synaptic strength between the multisensory neuron and the unisensory neurons are different according to each modality. The weights of the synapses that connect the tactile neurons and the multisensory neuron are all the same independent of the position of the neuron in the tactile area, according to Equations 2.4 and 2.5. W^t_{ij} and B^t_{ij} denote the weight of the feedforward and feeedback tactile synapses respectively. In turn, W^t_0 and B^t_0 represent the fixed value assigned to those synapses.

$$W^t_{ij} = W^t_0 \tag{2.4}$$

$$B^t_{ij} = B^t_0 \tag{2.5}$$

In contrast, the weights of the synapses that connect the auditory neurons and the multisensory neuron depend on the portion of auditory space that each neuron encodes with respect to the modelled skin portion of the hand. Thus, the synapses hold a constant weight for the space on and near the hand, covering 60 cm of the auditory space (20 cm for the hand and 40 cm for the space close to the hand). The synaptic weights outside this boundary (*Lim*) are described by a bi-exponential function decreasing with the distance between the neurons' RF and the hand, as shown by Equations 2.7 and 2.6. W^a_{ij} and B^a_{ij} denote the weight of the feedforward and feeedback auditory synapses respectively.

$$W^a_{ij} = \alpha \cdot W^a_0 \cdot exp\left(-\frac{D_{ij}}{k_1}\right) + (1-\alpha) \cdot W^a_0 \cdot exp\left(-\frac{D_{ij}}{k_2}\right) \tag{2.6}$$

$$B_{ij}^{a} = \alpha \cdot B_{0}^{a} \cdot exp\left(-\frac{D_{ij}}{k_1}\right) + (1-\alpha) \cdot B_{0}^{a} \cdot exp\left(-\frac{D_{ij}}{k_2}\right) \tag{2.7}$$

In both equations, the distance D_{ij} is equal to zero for the auditory neurons that encode the first 60 cm of the auditory space, whilst for the neurons outside this boundary D_{ij} is the minimum Euclidean distance between its RF centre and this boundary. W_0^a and B_0^a denote the value of the feedback and feedforward synapses respectively when D_{ij} is equal to zero. k_1, k_2 and α are parameters governing the exponential decay of synaptic weights of auditory neurons encoding regions outside the near space of the hand. The values assigned to these later parameters were selected to produce a fast decay immediately outside this space and a low decay afterwards, as in the original publication [40]. The feedforward and feedback auditory synaptic weights are shown in Figure 2.5.

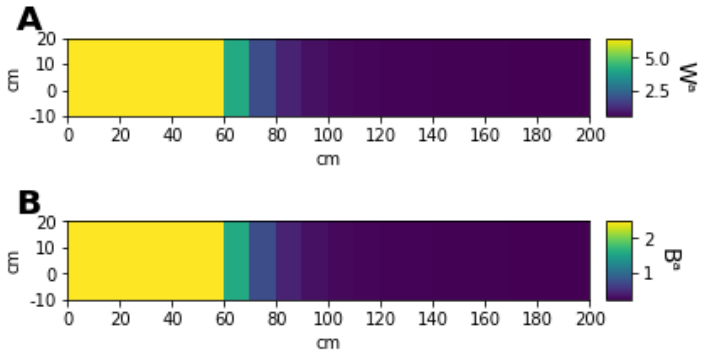

Figure 2.5: Bottom-up and top-down connections between the auditory area and the multisensory area. **Figure A** and **Figure B** show feedforward (W^a) and feedback (B^a) auditory synapses respectively. The colours represent the strength of the synaptic connections into neurons encoding the auditory area. The images illustrate stronger synapses towards neurons encoding the space close to the hand and exponentially weaker ones outside this region.

Overall, the design of the network aims to capture the observation that a multimodal stimulus (auditory and tactile) reinforces the perception of unimodal stimuli in unisensory areas. This occurs because the stimulus in one modality (e.g. auditory) reciprocally affects activation in the other unisensory area (e.g. tactile) due to the feedback synapses. Thus, the multisensory neuron resembles the responses of multisensory neurons located in posterior parietal areas of the primate brain which respond to tactile stimuli in the body and to auditory stimuli presented close, but not far from the body [29, 68]. Moreover, this area would mimic a portion of human multisensory regions in

the superior parietal, temporo-parietal and PMv that encode the representation of body part specific PPS [36, 34].

2.2.3 Network activity

The model is composed of non-spiking (rate) neurons, whose output is a continuous variable representing the neuron's firing rate. Each neuron of the model responds to its overall input through first-order temporal dynamics and a sigmoidal transfer function. The unisensory neurons temporal dynamics are defined in equation 2.8:

$$\tau \frac{dq_{ij}^{s}(t)}{dt} = -q_{ij}^{s}(t) + u_{ij}^{s}(t), \qquad s = t, a \tag{2.8}$$

In equation 2.8, $q_{ij}^{s}(t)$ stands for the state variable of a neuron at a given time step. This is affected by $u_{ij}^{s}(t)$, which denotes the overall input of a neuron at a given time step. Briefly, this input is the sum of the external stimulation received convolved with its RF, the recurrent input received from other neurons of its same area and the feedback input of the multisensory area (see Appendix A.2 for details). In this temporal relationship, τ is the time constant of the differential equation and its value is set according to the original publication [40], in agreement with realistic membrane time constants reported in the literature [69].

The unisensory neurons activity z_{ij}^{s} is computed out of the state variable $q_{ij}^{s}(t)$, as shown in equation 2.9:

$$z_{ij}^{s}(t) = \Psi\left(q_{ij}^{s}(t)\right) \cdot H\left(\Psi\left(q_{ij}^{s}(t)\right)\right), \qquad s = t, a \tag{2.9}$$

Equation 2.9 displays a sigmoidal function Ψ being applied to the state variable $q_{ij}^{s}(t)$. The result of this is multiplied by a Heaviside function H to avoid negative values in the activity of neurons. Finally, the sigmoidal function Ψ is defined by equation 2.10:

$$\Psi\left(q_{ij}^{s}(t)\right) = \frac{f_{min}^{s} + f_{max}^{s} \cdot e^{\left(q_{ij}^{s} - q_{c}^{s}\right) \cdot r^{s}}}{1 + e^{\left(q_{ij}^{s} - q_{c}^{s}\right) \cdot r^{s}}}, \qquad s = t, a \tag{2.10}$$

Here, 2.10, f_{min}^{s} and f_{max}^{s} are the lower and upper boundaries of the sigmoid function. q_{c}^{s} is the central point of the sigmoid and r^{s} denotes the slope of the curve at the central point.

The multisensory neuron activity is defined by an analogous set of equations (see Appendix A.3 for details) but with a substantial difference in the input received by the neuron. This input $u^m(t)$ is composed of the sum of the feedforward inputs from both auditory and tactile areas, as presented in equation 2.11.

$$u^m(t) = \sum_{i=1}^{N^t}\sum_{j=1}^{M^t} W_{ij}^t \cdot z_{ij}^t(t) + \sum_{i=1}^{N^a}\sum_{j=1}^{M^a} W_{ij}^a \cdot z_{ij}^a(t) \tag{2.11}$$

Here, 2.11, $z_{ij}^s(t)$ (s = t,a) denotes the activity of neuron *ij* in its respective unisensory area *s*. This is obtained by equations 2.9, 2.10 and 2.11. In addition, W_{ij}^s (s = t,a) represents the feedforward synapses from the unisensory neuron *ij* in the area *s* to the multisensory neuron. These synapses were introduced in the previous subsection and displayed in Figure 2.5A.

A couple of remarks must be considered before concluding this subsection. First, all the aforementioned differential equations were solved numerically employing the Euler integration method with a discrete time step of 0.4 ms, as in the original implementation [40]. Second, as highlighted by the authors of the original model [61, 45], each neuron of this network must not be interpreted as a single cell only but as the average behaviour of a group of cells that approximately share the same RF and code for a similar stimulus location. A similar interpretation must be held for the synapses among the neurons of the network: they do not represent a single synaptic connection but a summary of the overall synaptic strength of a group of neurons.

2.2.4 Network stimuli

Network stimuli was built for both unisensory areas to resemble the stimulation received by participants in the experiment described in Section 2.1. Both auditory and tactile stimuli had their centres located at a specific coordinate of their respective unisensory area. These inputs were implemented by a bidimensional Gaussian function I^s, as defined in equation 2.12. In contrast to the original implementation [40], we opted to exclude the random noise introduced in the stimulus intensity to avoid unexplained network variability [1].

$$I^s(x,y) = I_0^s \cdot exp\left(-\frac{\left(x_0^s - x\right)^2 + \left(y_0^s - y\right)^2}{2 \cdot \left(\sigma_I^s\right)^2}\right), \qquad s = t,a \tag{2.12}$$

[1] This change causes the model to be fully deterministic and be influenced only by the previously described network mechanics.

Here, I_0^s denotes the intensity of the stimulus. x_0^s and y_0^s are the coordinates of the central point of the stimulus applied in the unisensory area s. σ_I^s represents the spatial of the stimulus and was given a small value to simulate localised stimuli.

The tactile stimuli was always applied at coordinate x^t = 10 cm and y^t = 5 cm. In contrast, the auditory stimuli was always applied at coordinate y^a = 5 cm but the x^a coordinate changed across trials to simulate the presentation of the sound stimuli at different distances from the hand. Figure 2.6 shows an example of the tactile stimuli employed at every trial and an auditory stimuli presented at 80 cm from the hand (y^a = 100 cm).

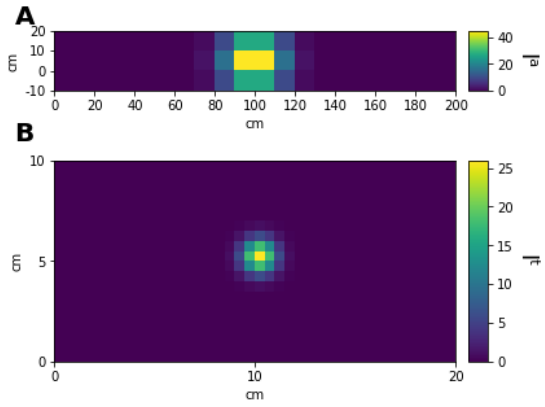

Figure 2.6: Network stimuli. **Figure A** and **Figure B** show tactile (I^t) and auditory (I^a) stimuli respectively. The colours indicate the intensity of the stimulus along the encoded tactile or auditory area.

2.2.5 Network basic functioning

The network functioning was tested by unisensory (sound only) and multisensory (audio-tactile) stimulation trials, as in the original implementation [40]. For both conditions the sound stimulation was applied at 15 equally spaced distances from the hand. The stimulation lasted 400 ms and was presented a single time at each position.

The network was evaluated first under unisensory sound stimulation. The steady state (i.e. the state of the multisensory neuron at the last time step) of the multisensory neuron was registered at every distance point from the hand. Results presented in Figure 2.7A show that the multisensory neuron steady state activity decreases outside the space close to the hand (40 cm) and rapidly reaches inactivation states. This behaviour is consistent with the results of the unisensory stimulation of the network presented in the original publication [40].

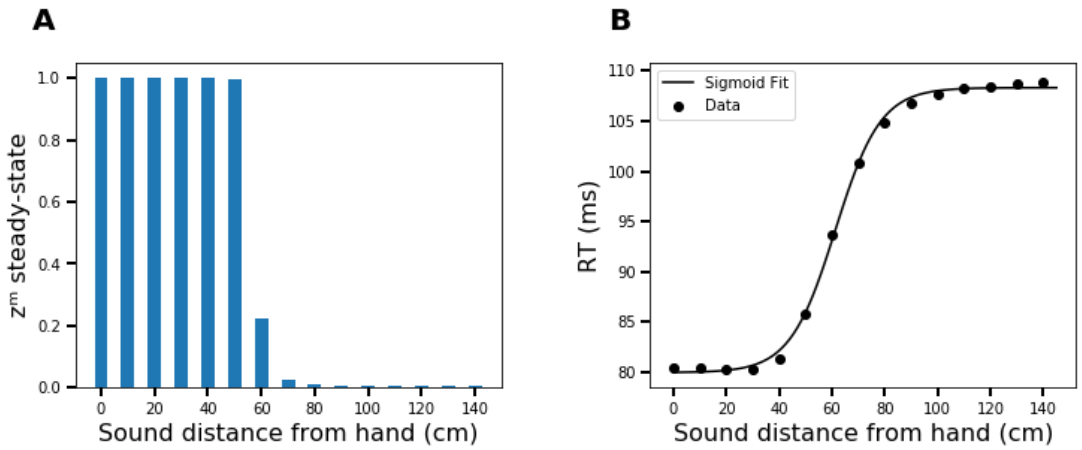

Figure 2.7: Evaluation of network activity. **Figure A** show the steady-state activity of the multisensory neuron. The plot shows a dramatic change in the activity of the multisensory neuron when the auditory stimulus is presented outside the near space from the hand. **Figure B** shows the network RT to multisensory stimulation across distance points. RT are depicted as dots, whereas a sigmoid curve fit is presented as a line. The plot shows faster responses of the network when the stimuli is administered close to the hand.

Next, the network was evaluated under multisensory stimulation, roughly resembling the behavioural paradigm of PPS measurement [38]. The reaction time (RT) of the network was registered at every distance point as the time at which the tactile area reached the 90% of its final activation state. Figure 2.7B shows the results of this simulation.

The RT obtained show that the tactile area activates faster when the auditory stimulus is presented close to the hand, mimicking what has been observed in behavioural studies [38]. Results of the fitting procedure (see Appendix A.4 for details) reveal that the curve's average central point is located at 61cm from the hand (coordinate y^a = 81 cm in the auditory area) and present a slope of 0.11, which is in agreement to what was reported in the original publication [40].

2.3 Experiment simulation in the network

This experiment was simulated computationally by holding relevant assumptions. First, it was assumed that the perceived velocity of the sound was 30 cm/s. Although the exact value of the velocity of sound was not reported in the aforementioned study [4],

further studies employing the audio-tactile paradigm have reported velocities ranging from 22 cm/s to 35 cm/s [39]. For the simulations performed in this study, a speed of 30 cm/s was selected because it accurately elicited PPS representations similar to the ones observed in healthy controls.

Second, both auditory and tactile stimulation employed to stimulate the network were not realistic in terms of their physical properties (e.g. duration and magnitude). The network stimuli employed for the experiment simulation were the ones described in section 2.1.5. The stimulation was configured to last 200 ms for both auditory and tactile stimuli, because the model was not designed to operate with realistic time magnitudes of tactile stimulation [40].

Third, the experiment simulation assumed that the participants were stimulated at more than five distance points to obtain a better accuracy of the PPS representation generated by the model. Specifically, the simulation evaluated RT at delays from 300 ms to 2700 ms at intervals of 100 ms, which covered 25 distance points between 39 cm and 111 cm from the hand.

Fourth, it was assumed that the network model does not capture the entire neural process that causes the motor responses (i.e. button pressing) examined in the task. The scale of network RT does not match exactly with RT found in human participants, as can be observed in the multisensory condition testing presented in Figure 2.7. This discrepancy is assumed to be related to instances of sensory processing that the model does not register, such as low-order neural structures of both the auditory and somatosensory pathways. Hence, the RT produced by the model is a rough measure of tactile sensitivity that does not consider the sensorimotor processing required to press a button. To match RT data observed in experiments, a linear regression is computed after every run of the model (see Section 2.5 for more details).

Fifth, the original parameter values that define the feedforward and feedback auditory synaptic weights (see Equations 2.7 and 2.6) outside the space near the hand were manipulated. Specifically, the model was fitted to the average RT registered in the HC group [4] to obtain values of k_1, k_2 and the boundary (Lim) that defines the near space from the hand (see Section2.5 for details on the fitting procedure). The purpose of this manipulation was to fine-tune the model to reproduce PPS representations of healthy individuals that closely resemble the ones observed in the empirical study. Hence, in the following this network setup will be denominated HC model and will be taken as the baseline to examine the influence of SCZ and H-SPQ in the network (see Section 2.4).

A single simulation of the experiment under these considerations is presented in Figure 2.8A. The average RT values at each distance point were fitted to a sigmoid function (see Appendix A.4) to calculate the central point and the slope of the PPS representation. The simulation showed that the PPS representation generated by the HC model has its CP located at 63 cm from the hand and presents a slope of 0.9 (see Figure 2.8A). A further exploration of the model mechanics is described in Figures 2.8 B, C and D. In short, the mechanics depiction illustrates how the RT of the network are influenced by the activity of the multisensory neuron, which in turns depends on the distance of the sound stimulation.

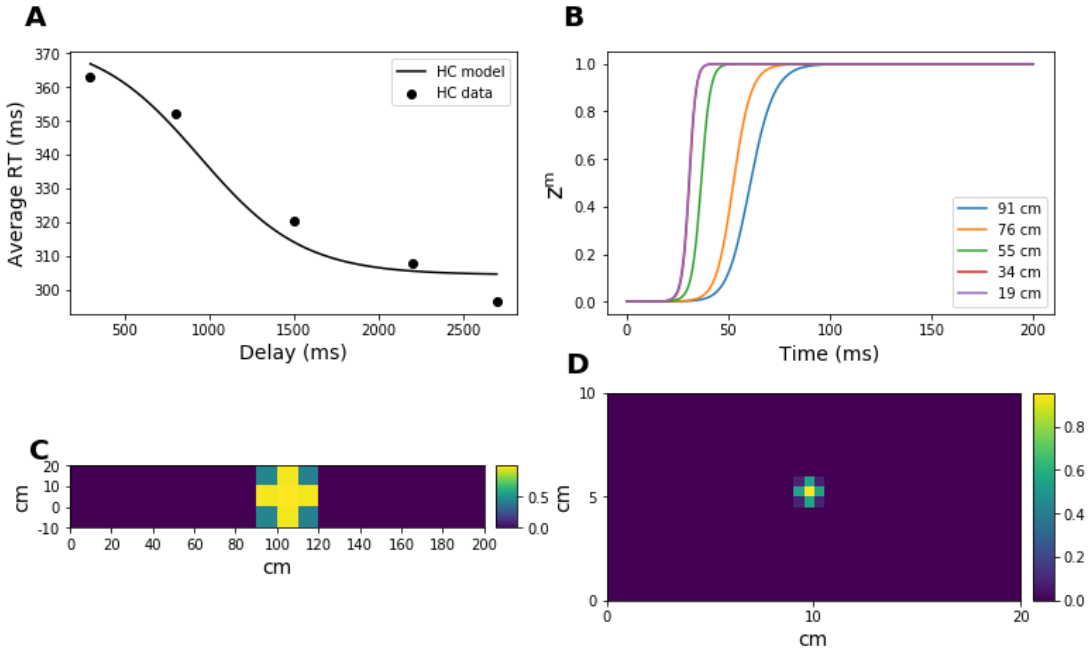

Figure 2.8: Mechanics of the HC network model. **Figure A** shows a close match between the PPS representation generated by the network and the average RT of the HC group. **Figure B** presents the time dependent activity of the multisensory neuron across the distances evaluated in the empirical study. The plot indicates a faster activation of the multisensory neuron when the sound stimulation is presented closer to the hand. **Figure C** and **Figure D** show the steady-state activity of the auditory and tactile neurons respectively. The images illustrate that the network activity closely corresponds to the administered stimuli (refer to Figure 2.6 for a comparison).

2.4 Modelling the influence of SCZ and H-SPQ in the network

Until this point, the original implementation of the model was replicated and adapted to account for the empirical data observed in healthy participants. This setup will be considered as a starting point to introduce impairments in the model with the purpose of accounting for PPS representations observed in SCZ and H-SPQ [4]. More precisely, we aim to detect what impairments cause the size reduction of the PPS and the sharpening of its boundary.

For this purpose, we ought to evaluate two consistently observed impairments in the SCZ spectrum: E/I imbalance [11] and synaptic density decrease [26]. Particularly, we aim to explore the effects of modulating the E/I balance of recurrent connections in both unisensory areas. Similarly, we intend to examine the effects of decreasing the density of feedforward and feedback synapses in both unisensory areas.

Overall, we aim to answer the following questions: Is the E/I modulation related to the size of the PPS? What is the influence of top-down and bottom-up decreased synaptic density in the encoding of the PPS? Are both impairments required to reproduce PPS representations observed in SCZ patients and H-SPQ individuals?

2.4.1 Modulation of the E/I balance

The modulation of the E/I balance is implemented in the model by inducing disinhibition or excitability reduction in the unisensory areas. This approach is inspired by what has been successfully implemented in working memory models of SCZ using biologically realistic networks (i.e. based on integrate-and-fire neurons) [9, 10]. In those models, an imbalance of E/I was achieved by impairing NMDA synapses in inhibitory interneurons or excitatory neurons, which respectively reduces inhibition or excitability in the network. However, this cannot be implemented in the PPS network model because it is not built on integrate-and-fire neurons and does not include inhibitory interneurons in its structure.

We propose an alternative implementation of the E/I imbalance suitable for this network model based on previous research [6, 70]. This approach induces inhibition by uniformly shifting the response curve of the neurons activation function to the right and induces excitation by shifting such curve to the left. We implemented this by introducing a bias term (β) in the sigmoid activation function of both auditory and

tactile neurons, as shown in equation 2.13:

$$\varphi\left(q_{ij}^{s}(t)\right) = \frac{f_{min}^{s} + f_{max}^{s} \cdot e^{\left(q_{ij}^{s} - q_{c}^{s}\right)\cdot r^{s} + \beta}}{1 + e^{\left(q_{ij}^{s} - q_{c}^{s}\right)\cdot r^{s} + \beta}} \qquad s = t, a \tag{2.13}$$

The notation used in this function is the same as that in equations 2.9 and 2.10. In such sigmoidal relationship, the term β denotes the bias introduced to modulate the E/I balance in the unisensory areas. β can reduce inhibition by adopting positive values (β +) or reduce excitability by adopting negative values (β -). Although less biologically detailed, this implementation is able to reproduce reductions in inhibition or excitability in the unisensory areas, as observed in the steady-state activity[2] of tactile neurons displayed in Figure 2.9.

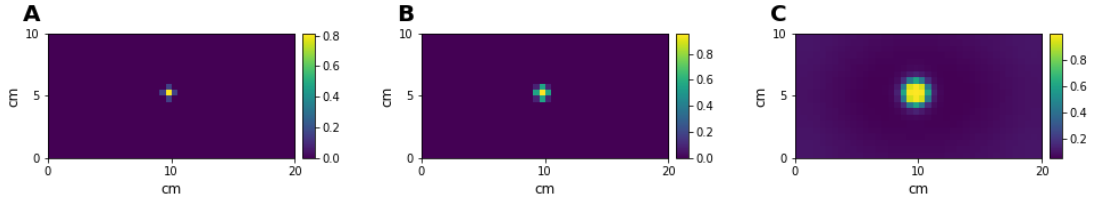

Figure 2.9: E/I balance influence in steady-state tactile activity. **Figure B** presents the activity of tactile neurons under E/I balance ($\beta = 0$). **Figure A** and **Figure C** show tactile activity under excitability reduction ($\beta = -1.5$) and disinhibition ($\beta = 4.5$) respectively. The images represent the area of the hand that is encoded and the colours indicate the firing rate of the neurons encoding portions of the tactile area. These figures illustrate how the neural activity can be compressed (left) or spread beyond the point of stimulation (right) by the E/I balance modulation.

In the excitability reduction condition (Figure 2.9A) it can be observed that only the neurons that encode the specific coordinate of the centre of the tactile stimulus were active and registered lower rates than in the balanced condition (Figure 2.9B). In contrast, in the inhibition reduction condition (Figure 2.9C) it can be observed that the activation of tactile neurons spreads beyond the centre of the tactile stimulus and registered higher rates than in the balanced condition.

The effects of the modulation of E/I balance in the PPS representation generated by the network model will be explored through a parameter sweep. For this purpose, β values ranging from 0 to 4.5 will be explored to examine the effects of disinhibition

[2]The steady state activity of a tactile neuron is defined as the activity registered in the last time step of the simulated experiment.

in the unisensory areas. Similarly, β values ranging from 0 to -1.25 will be explored to examine the effects of excitability reduction in the unisensory areas. Values outside these ranges were excluded from the sweep because the PPS representation generated by these values ceases to resemble a sigmoid curve, which is characteristic of the average PPS representations found in the literature for HC, SCZ, L-SPQ and H-SPQ [4].

2.4.2 Effects of decreasing synaptic density

The decrease of synaptic density in bottom-up and top-down connections is implemented in the model by weakening feedforward and feedback synapses between the unisensory areas and the multisensory area. A pruning procedure inspired by the concept of neural Darwinism [71] (which proposes that neurons compete for access to other neurons) is employed. This is consistent with the observation that less robust connections tend to be pruned away [72]. This concept can be implemented in neural network models by assuming that weaker and stronger connections in the model (in terms of synaptic weights) represent fewer and larger number of synapses respectively, as performed in [5, 6, 70].

In line with such implementations, the pruning procedure employed in this study consisted in re-setting the connection weights of both tactile and auditory top-down and bottom-up synapses that were below a certain threshold ρ to zero. The impact of the pruning in the feedforward and feedback synapses was calculated by dividing the sum of the weights of the pruned connections over the total sum of the weights of the connections before pruning[3]. An illustration of the pruning effects in the synaptic weights of top-down connections to the auditory area is presented in Figure 2.10.

This illustration shows the weights of feedback auditory synapses after implementing four different pruning levels. It can be observed that at low levels of pruning (Figures 2.10 A and B), the exponential decay of the synaptic weights values outside the near space of the hand (yellow) is roughly preserved (see Figure 2.5B for comparison). In contrast, at high levels of pruning the synaptic weights distribution outside the near space of the hand is either heavily distorted (Figure 2.10C) or set to zero (Figures 2.10D).

The effects of decreasing synaptic density in bottom-up and top-down connections will also be explored through a parameter sweep. Since a given pruning level could be

[3]Since feedforward and feedback auditory synaptic weights are in a different scale, *rho* was defined proportionally to achieve the same percentage of pruned synapses in both type of connections.

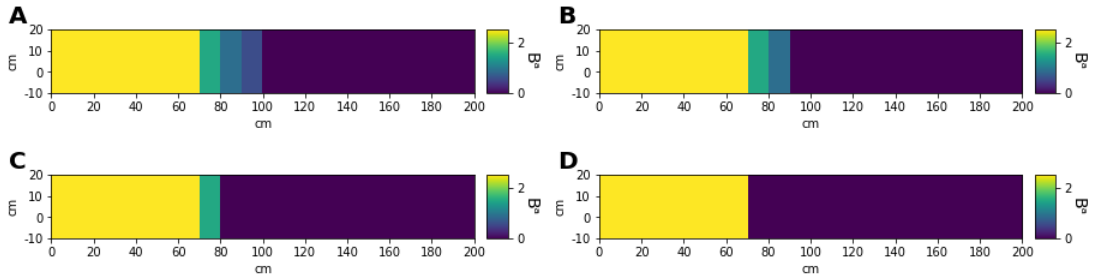

Figure 2.10: Feedback auditory synapses (B^a) after pruning. **Figures A, B, C and D** show the distribution of synaptic weights at pruning levels of 11.39%, 13.92%, 17.83% and 24.35% respectively. The images represent the area of the auditory space that is encoded by auditory neurons. The colours correspond to the strength of the synaptic connection to the neurons encoding the auditory space. The images reveal that synapses outside the near space (yellow) are progressively impaired as the pruning level increases.

achieved by different nearby thresholds (see Appendix B.1 for details), discrete values of ρ that lead to different pruning levels were considered. Hence, the effects of the pruning levels presented above (applied to both feedforward and feedback synapses simultaneously) were explored.

2.5 Fitting procedure

The RT generated by the network were fitted to the experimental data of the study introduced in Section 2.1 [4]. First, the aim of the fitting was to find the values of k_1, k_2 and (Lim) to match the RT generated by the network and the average RT data of the HC group. Second, the fitting aimed to find the values of β and ρ that produced the best match of the RT generated by the model and the average RT data of the SCZ, L-SPQ and H-SPQ groups.

A fitting procedure inspired in an already established method for parametrisation of connectionist models [73] was employed [4]. The procedure used in this study consisted of matching the time units of the model and the experiment and minimising a cost function with an optimisation algorithm. At every iteration of the minimisation routine, the RT were matched by a standard linear regression, as presented in Equation 2.14.

[4]The main difference between the original method and our procedure is that we omitted the steps aimed to deal with variability in network models because our network generates deterministic responses.

$$RT^{data} = a \cdot RT^{model} + b \tag{2.14}$$

Here, RT^{data} and RT^{model} represent the RT obtained in the empirical study and the simulated experiment respectively. Parameters a and b represent the slope and the intercept of the linear relationship.

Next, the cost function defined by Equation 2.15 was calculated.

$$Cost = \sum_{i=1}^{N} \left(\frac{RT_i^{data} - RT_i^{model}}{RT_i^{data}} \right)^2 \tag{2.15}$$

Here, RT_i^{data} and RT_i^{model} denote the RT measured at the ith distance point. N represents the number of distances measured (i.e. 5 in the empirical study). This cost function was minimised by a stochastic algorithm called Differential Evolution [74]. Such algorithm was chosen because gradient based techniques failed to minimise the function due to the previously mentioned behaviour of parameter ρ (see Appendix B.1 for details). The bounds given to the algorithm to find k_1, k_2 and *Lim* were (0, 100), (500, 1000) and (20, 80) respectively. In addition, the boundaries employed to find β were the same as the ones considered for the parameter sweeps. The boundaries defined for *rho* allowed pruning levels between 0% and 24.35%.

Chapter 3

Results

3.1 PPS representation under E/I modulation and decreased synaptic density

A detailed description of the computed parameter sweeps for E/I balance modulation (β) and pruning (ρ) is presented in Appendix C.1 and C.2. The simulations revealed that disinhibition (β +) reduces the size of the PPS representation generated by the model, whereas excitability reduction (β -) increases its size. In contrast, the decrease of synaptic density in feedforward and feedback connections influences both the size and the slope of the PPS. Specifically, the increase of the pruning level reduces the size of the PPS and sharpens its boundary (i.e. causes the slope of the PPS representation to be steeper). An exploration of the interaction of both parameters is presented in this section.

The combined effect of inhibition reduction and decreased synaptic density on PPS representation is shown in Figure 3.1. Results in the top panel overall indicate that slopes are more steeped as the pruning level increases and that disinhibition reduces the effects of pruning on the steepness of the PPS representation. The bottom panel indicates that the size of the PPS decreases as the pruning gets more intensive and that disinhibition increases the effect of pruning on the size of the PPS. An exploration of the combined effect of excitability reduction and decreased synaptic density is included in Appendix C.3.

In sum, the simulations presented in this section suggest that both E/I modulation and decreased synaptic density are relevant to reproduce PPS representations observed in the SCZ spectrum. The PPS representation observed in H-SPQ (characterised for

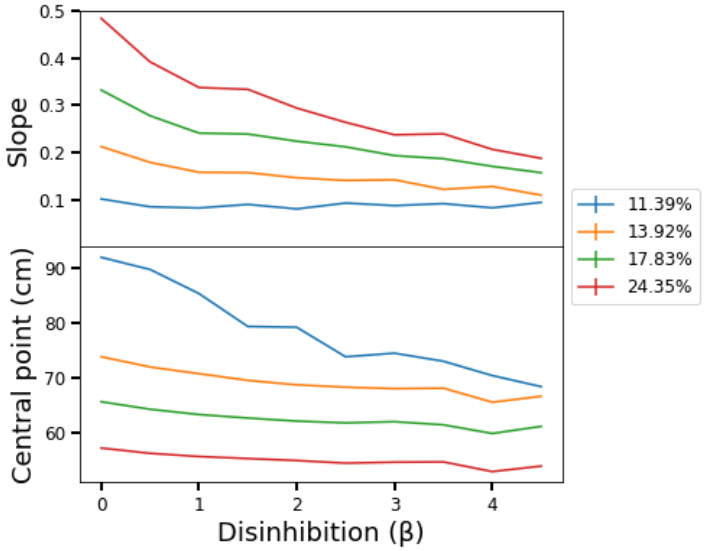

Figure 3.1: Effect of inhibition reduction and decreased synaptic density in PPS. Coloured lines depict the features (i.e. slope and size) of the PPS representation generated by the model at different levels of inhibition reduction. Different lines represent the features generated by the model at different pruning levels, as indicated in the legend. Disinhibition modulates the effects of pruning by reducing the steepness and the size of the PPS representation.

being small) is possibly related to disinhibition (β +) in unisensory areas. In contrast, the PPS representation observed in SCZ (characterised for being small and sharply defined) is expected to be caused by the interaction of both E/I balance modulation and pruning. The exact values of the parameters that give rise to these representations are presented in the following section.

3.2 Identification of SCZ and H-SPQ network models

The results of fitting the model to the average RT data of the SCZ, H-SPQ and HC groups are presented in Table 3.1 and Figure 3.2. Results shown in Table 3.1 suggest that the network requires strong disinhibition in the unisensory areas to generate PPS representations that match the average RT data of both SCZ and H-SPQ groups, whilst the HC group requires only a weak disinhibition. Furthermore, the network requires a strong pruning to reproduce the PPS observed in SCZ, whereas weak or no pruning is required to match the representation observed in H-SPQ and HC (see Figure 2.10 for an illustration of the different pruning levels).

	Network		Linear Regression	
	β	**Pruning (%)**	**a**	**b**
HC	0.63	4.79	5.17	-73.54
SCZ	4.49	24.35	14.13	-252.58
H-SPQ	4.30	0	14.73	-455.32

Table 3.1: Parameters obtained by the fitting procedure.

The parameters obtained for the linear regression model indicate that the slope (a) of the linear relationship required to be steeper to fit SCZ and H-SPQ in comparison to HC. This indicates effect that increased excitability has in the differences of RT across the evaluated distances [1]. The intercept (b) increased in absolute terms to fit the data of both SCZ and H-SPQ groups. This increment compensated the previously mentioned increase in a to display RT in the scale observed in the experiment [2].

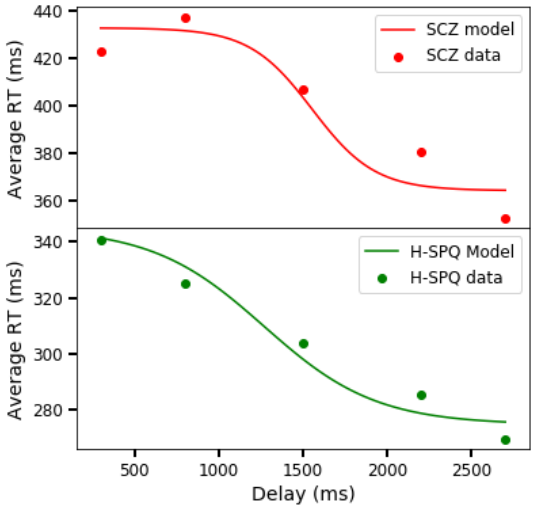

Figure 3.2: PPS representations generated by the SCZ and SPQ network models identified by the fitting procedure. The coloured lines depict the sigmoid fit obtained out of the data generated by the SCZ model (red) and the H-SPQ model (green). The coloured dots represent the average RT obtained in the empirical study for the aforementioned populations.

Overall, the results presented in this section reveal that the network model is able to

[1] In other words, the inter-distance variability of the RT generated by the model at default conditions is not preserved. It must be noted, however, that such original variability does not correspond to the variability observed in experimental data either, as the slope obtained for HC controls (a = 5.17) suggest.

[2] Such compensation was less intensive for SCZ patients because their RT in the experiment were slower than in HC and H-SPQ individuals. This occurs possibly due to the effects of medication.

generate PPS representations that resemble the average PPS observed in SCZ patients and H-SPQ individuals (see Figure 3.2). Although the network model is not able to reproduce RT in the scales observed in experimental conditions (i.e. requires a linear regression model for this purpose), it is able to capture the shapes of the PPS of both populations and resemble the reports of the empirical study [4]. Specifically, the PPS generated by the SCZ model is represented by a sigmoid function with central point at 53 cm (1556 ms) from the hand and a slope of .17, whereas the PPS generated by the H-SPQ model is represented by a sigmoid with central point at 62 cm from the hand (1262 ms) and a slope of .09 [3].

In the following sections, the identified models are explored to generate predictions regarding the symptoms observed in the SCZ spectrum.

3.3 Exploration of the SCZ and H-SPQ network models

3.3.1 Mechanics of the SCZ and H-SPQ models in the simulated experiment.

An exploration of the mechanics of the models in the simulated experimental paradigm is presented in Figures 3.3 and C.5.

Results of the SCZ model shown in Figure 3.3A reveal that the multisensory neuron activates faster and its dynamics remain constant across the evaluated sound distances (see Figure 2.8B for a comparison with the HC model). Figures 3.3 B and C indicate that the network activity spreads beyond the coordinates at which the stimulus was delivered. Such spread of activation occurs due to recurrent (colours yellow and green) and feedback synaptic inputs. This latter input influence may be observed in the weak activity registered in the first 60 cm of the auditory area (blue).

Results for the H-SPQ model reveal similar mechanics to those observed in the SCZ model (see Appendix C.4.1 for an illustration). The key difference is that the spread of activation in unisensory areas is dominated by the input of recurrent connections and is limited to regions that are near to the point where the stimulus was administered.

In sum, the results presented in this subsection reveal that the SCZ and H-SPQ models present similar dynamics mainly characterised by the influence that disinhibition in unisensory areas produces in the network. Contrary to the mechanics observed

[3] The location of the central point expressed in ms is an approximation based on the assumption of the velocity of sound.

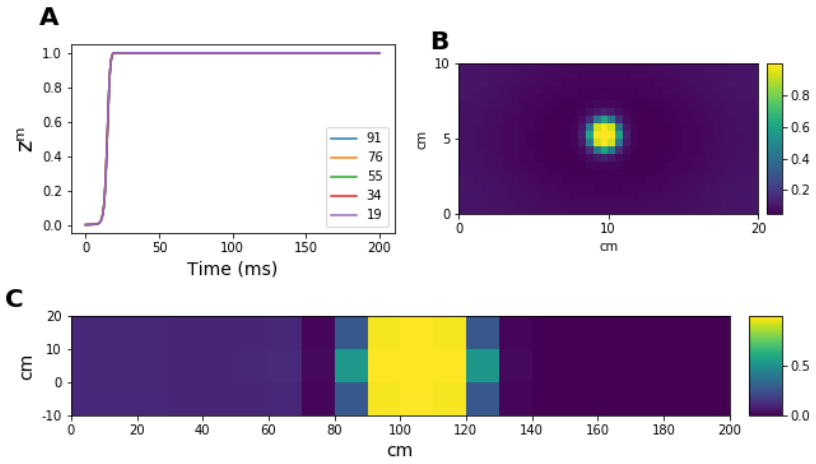

Figure 3.3: SCZ network mechanics under audio-tactile stimulation. **Figure A** shows the activity of the multisensory neuron under auditory and tactile stimulation. The different colours represent the distances at which the sound stimulation was administered. **Figures B and C** show the steady state activity of the tactile and auditory areas respectively. The colours represent the firing rate of the neurons that encode a given coordinate of the unisensory areas. The images reveal that there is no difference in multisensory activity across the evaluated distances and that unisensory activity spreads beyond the coordinates at which the stimulus was delivered.

in the HC model, audio-tactile stimulation in the SCZ and H-SPQ networks produces a faster activation of the multisensory neuron and a widespread activity in unisensory areas beyond the coordinates at which the stimuli are administered. The main difference between the models is that the SCZ network displays weak spontaneous activity in the auditory area close to the hand.

3.3.2 Mechanics of the SCZ and H-SPQ models under auditory stimulation.

The mechanics of the models under auditory stimulation were examined according to the the procedure described in Section 2.2.5. Results of this exploration are presented in Figures 3.4 and 3.5.

Results in Figure 3.4A indicate that the multisensory neuron of the SCZ network reaches its maximum level of activation irrespective of the distance at which the sound is delivered. Figures 3.4C and D display spontaneous activity in both auditory and tactile areas. Figure 3.4C shows weak activity registered in the first 60 cm of the auditory

area even though the stimulus was administered at 160cm. Figure 3.4D indicates weak activity in the tactile area in spite of the absence of tactile stimulation.

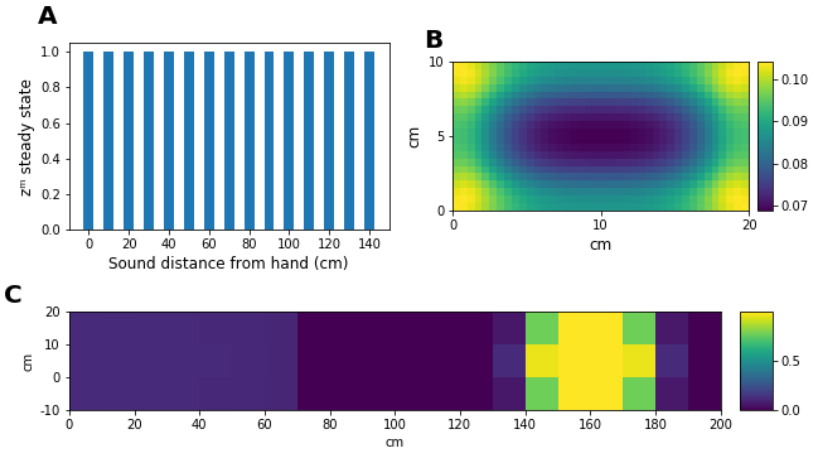

Figure 3.4: SCZ network mechanics under auditory stimulation. **Figure A** shows the steady state activity of the multisensory neuron under auditory stimulation administered at different distances from the hand. **Figures B and C** show the steady state activity of the tactile and auditory areas respectively. The colours represent the firing rate of the neurons that encode a given coordinate of the unisensory areas. The images reveal that there is no difference in multisensory steady-state activity across the evaluated distances and that spontaneous activity is registered in both areas.

Results of the H-SPQ model shown in Figure 3.5 reveal mechanics different to those observed in the SCZ model. Figure 3.4A indicates that the multisensory neuron of the H-SPQ network reaches its maximum level of activation when the sound is administered up to 90 cm from the hand, which is 20 cm further than the PPS boundary observed in the HC model. In addition, Figures 3.4C and D show the presence of a very weak spontaneous activity only in the tactile area.

The results presented throughout this subsection reveal that the SCZ and H-SPQ models are impaired in their ability to properly encode the PPS space as the space close to the hand. Although their PPS representations are smaller (53 cm and 62 cm respectively), their multisensory neurons respond to sensory stimulation administered beyond the boundary of 72cm observed in the HC model. Such anomalous multisensory activity produces weak spontaneous activity in the unisensory areas as a result of the feedback input of the multisensory neuron, particularly in the SCZ network.

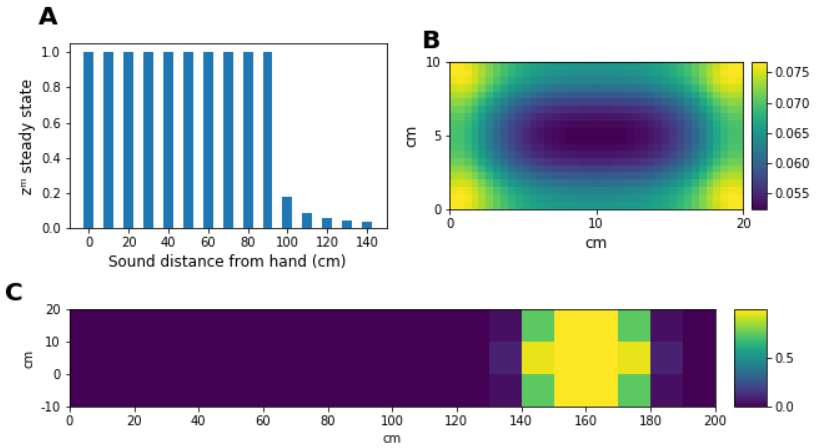

Figure 3.5: H-SPQ network mechanics under auditory stimulation. The description of **Figures A, B and C** is the same as those in Figure 3.4. The images reveal that multisensory neuron activates when the sound is presented up to 90 cm from the hand and that spontaneous activity is registered in the tactile area.

3.3.3 Two-point discrimination in the SCZ model

The effects of disinhibition in unisensory areas were further explored under two-point tactile stimulation. We simulated the administration of two tactile stimuli separated by 2 cm in the modelled hand. The registered tactile activity in the HC and SCZ models is presented in Figure 3.6. Results of the simulation reveal that tactile activity in the SCZ model is distorted and does not clearly distinguish between the two stimuli. In contrast, tactile activity generated by the two stimuli do not overlap in the HC model.

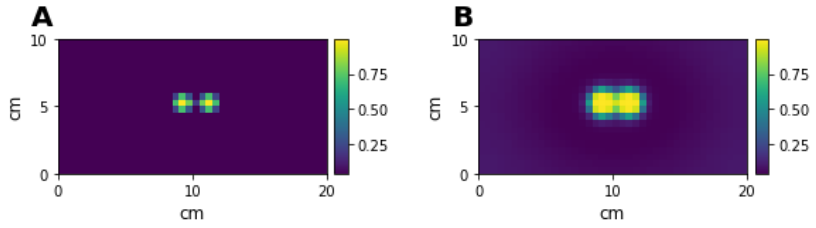

Figure 3.6: Tactile activity during two-point tactile stimulation. **Figures A and B** represent the steady-state tactile activity registered during two-point stimulation in the HC and SCZ models respectively. The images represent the encoded area of the modelled hand and the colours indicate the firing rate of the neurons that encode a given coordinate of this area. They illustrate how tactile activity generated by the stimuli overlaps in the SCZ model.

Chapter 4

Discussion

This study aimed to model the neural mechanism that gives rise to the PPS representations observed in SCZ patients and H-SPQ individuals. For this purpose, an already existing network model of PPS [40] was modified in two aspects relevant for its mechanics: modulation of the E/I balance and pruning of feedforward and feedback synapses. These modifications represented the consequences of the hypofunction of NMDA receptors and GABA neurons together with elevated activity of the D_2 receptor, which are thought to be the origin of predictive coding impairments in contemporary computational accounts of SCZ [13, 14].

Exploration of parameter values (Section 3.1) and fitting to experimental data (Section 3.2) suggest two distinct parameterisations that give rise to the PPS representations observed in SCZ patients and H-SPQ individuals.

In the model, the PPS of H-SPQ individuals is characterised by an increased excitability of unisensory neurons responsible for the encoding of the spatial location of both auditory and tactile stimuli. Based on this computational evidence, it can be proposed that such increase in excitability causes the narrower PPS empirically observed in H-SPQ individuals (in comparison to L-SPQ individuals) [4].

In contrast, the PPS of SCZ patients in the model is characterised by a stronger increase of excitability of the aforementioned unisensory neurons along with a decrease of bottom-up and top-down synaptic density between unisensory and multisensory neurons. This computational evidence suggest that such stronger increase in excitability causes the smaller PPS observed in SCZ patients, whereas the decrease in synaptic density causes the sharply defined slope of the PPS representation registered in the same population [4].

4.1 A novel working model of PPS representation in SCZ spectrum disorders

Our findings oppose the current working model of PPS representation in SCZ. Particularly, they contradict the assertion that impairments in self demarcation are related to a shallower definition of the PPS boundary originated by weaker synaptic connections between multisensory neurons and unimodal neurons [3]. In contrast, we suggest that the reduction in the size of the PPS observed in SCZ and H-SPQ individuals is related to disinhibition of unisensory neurons that encode the spatial location of external stimuli. We also propose that the sharper definition of the PPS boundary (i.e. a steeper slope of the PPS representation) observed in SCZ is related to a decrease in feedforward and feedback synaptic density among unisensory and multisensory neurons.

This new model holds in spite of empirical evidence linking the shallowness of the PPS boundary and reports of unusual experiences after sensory deprivation [50]. In SCZ, a steep PPS boundary is compatible with a weaker self-demarcation because disinhibition of unisensory areas reduces the overall influence of feedforward and feedback synapses in the network mechanics, as shown in Sections 3.3.1 and 3.3.2. In other words, the resulting activity of the multisensory and tactile neurons is less dependent of the synaptic input received by bottom-up and top-down connections in the network. Hence, we propose that the sharpness the PPS boundary may be taken as an index of self permeability [3, 50] only when the E/I balance is granted.

Furthermore, this new model suggests the possibility to distinguish between schizotypy and SCZ regarding the encoding of the PPS. Although both are characterised by an E/I imbalance, we suggest that they differ in the degree of impairment of top-down and bottom-up synapses between unisensory networks and multisensory networks located in fronto-parietal areas [1]. In the model, we note such difference in the pruning levels observed in the SCZ and H-SPQ models (see Section 3.2. Hence, we propose that they differ in how decreased the synaptic density is among the aforementioned networks: the decrease in H-SPQ individuals is weak, whereas in SCZ patients it is strong.

A graphical representation of the novel working model of PPS representation in SCZ is presented in Figure 4.1. This figure shows the influence that the evaluated parameters (i.e. β and ρ) have in the PPS representation of SCZ patients (solid lines

[1] Such synaptic impairment is thought to be a consequence of failures in signalling across different levels of the cortical hierarchy produced by the E/I imbalance [13].

marked with an asterisk). Moreover, it presents predictions (dashed lines) regarding the influence of disinhibition in the personal space and tactile discrimination observed in patients. Finally, it shows how the aforementioned observations are related to symptoms and impaired functions associated with the SCZ spectrum according to previous research (solid lines). In the following sections, the proposed links between PPS, personal space and tactile discrimination are discussed in light of our findings and previous reports.

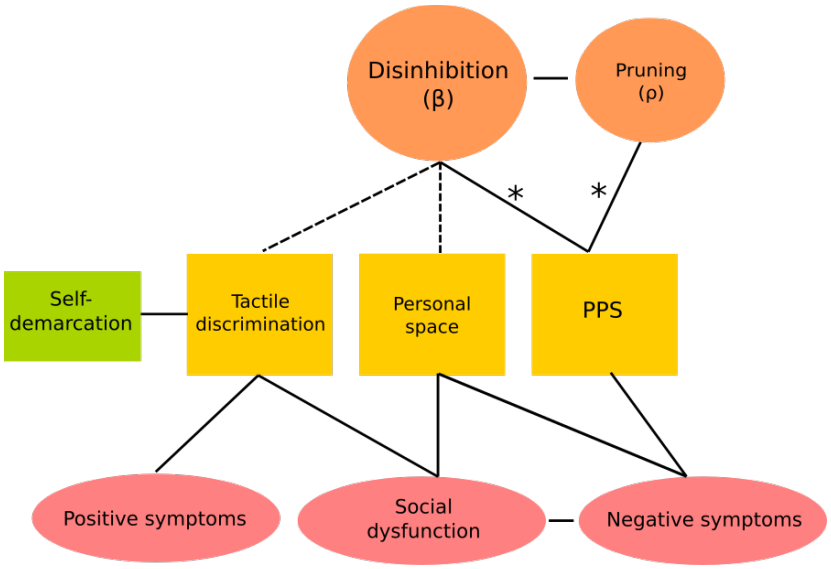

Figure 4.1: New working model of PPS representation in SCZ. Solid lines marked with an asterisk represent causal relationships observed in this study; solid lines represent links reported in the literature; dashed lines represent predictions based on the model mechanics. This figure illustrates how disinhibition and pruning influence behavioural observations of tactile discrimination, personal space, PPS and their associated symptoms.

4.2 Encoding of PPS and personal space delimitation in SCZ

Previous research has consistently shown that the personal space in SCZ patients is enlarged and correlated with negative symptoms [52, 53, 54, 55, 56, 57, 58]. However, the link between the enlargement of the personal space and the shrinking of the PPS observed in patients [4] is not well understood. We propose a new hypothesis to relate both observations based on the effects that disinhibition has in unisensory areas.

The exploration of the SCZ and H-SPQ network models under unisensory conditions (Section 3.3.2) revealed that the multisensory neuron failed to accurately encode the PPS as the space close to the modelled hand. This suggests that although the behaviourally measured PPS gets smaller, the PPS neurons of both H-SPQ individuals and SCZ patients encode a larger space compared to healthy controls. Moreover, these simulations (see Figures 3.4 and 3.5) showed that the combined effect of the over excitability of unisensory areas and the impaired encoding of the PPS neuron was able to produce spontaneous activity in tactile neurons and auditory neurons.

Based on these observations, we suggest that a stimulus (e.g. a person) presented far from the body of a SCZ patient elicits weak activity of neurons encoding the space on and close to her body. We also propose that such spontaneous activity contributes to the exacerbated feeling of intrusion of the personal space reported by patients [75]. Hence, the space perceived as "near" is extended and the distance at which SCZ patients feel comfortable with the presence of another individual (i.e. personal space) increases. Overall, this is congruent with the idea that the encoding of the PPS evolved as a mechanism to respond against treats from the environment [37] and evidence linking the encoding of the PPS and social interaction [76].

At the neurobiological level, interpersonal difficulties in SCZ have been related to cortical hypersensitivity. More precisely, it has been suggested that hyper-responsivity of fronto-parietal networks responsible for the sensory-motor coupling required for the initiation of behaviour is the origin of personal space enlargement, social dysfunction and negative symptoms [58]. Furthermore, recent studies show that over excitation of the right superior temporal cortex is correlated with the schizotypal trait named Social Disorganisation [2][78, 77].

Based on this evidence, we suggest that cortical disinhibition possibly produced by an impairment of GABA transmission or NMDAR hypofunction [11] causes PPS shrinking, social disorganisation, negative symptoms and personal space enlargement in SCZ (see Figure 4.1). Nevertheless, it must be considered that the size of the personal space is also mediated by cultural and individual factors, as well as brain activity specific of social stimuli processing (e.g. functional connectivity among premotor regions and both the midbrain periaqueductal gray and the intraparietal sulcus) [59, 60]. In addition, the specific relation among negative symptoms, social disorganisation and cortical hypersensitivity must be further clarified [51].

[2]This phenotype is present in both the autism and SCZ spectra. It clusters reports of social anxiety, constricted affect, social skills, communication, absence of close friends, odd speech and odd behaviour [77].

4.3 Encoding of PPS and tactile discrimination in SCZ

The features of the SCZ network model presented in this study (i.e. increased excitability in unisensory areas and decreased feedforward and feedback synaptic density) are compatible with reports of impaired tactile discrimination in the SCZ spectrum [79, 80, 81, 48]. More precisely, it has been reported that SCZ patients and their relatives require a larger distance to distinguish between two-point or one-point tactile stimulation in an experimental paradigm named two-point discrimination [3] [79].

In the model, such reduced tactile discrimination can be explained by disinhibition in unisensory neurons (see Section 3.3.3). Particularly, Figure3.6B illustrates how neuronal activity spreads beyond the coordinates at which tactile stimuli are administered due to the effect of failures in recurrent inhibition. Thus, tactile stimulation elicits the response of a group of neurons encoding a larger area than in normal conditions (i.e. E/I balance), and the distance required by the individual to distinguish between two different stimuli increases.

Furthermore, our results support the view that reduced tactile sensitivity is related to self-disturbances [1, 2] and failures in bodily self-consciousness [3]. Specifically, a reduced performance in the two-point discrimination task correlates with higher scores of the cognitive-perceptual factor (positive symptoms subscale) of the SPQ scale [80, 81] and the propensity to experience the Pinocchio Illusion (PI) [48]. In turn, the PI is correlated with positive symptoms, loneliness and the prevalence of reports of out-of-body experiences [48]. In this context, we predict that failures in cortical inhibition of networks that encode portions of the skin underlie the proneness of SCZ patients to experience self-aberrations as the ones examined in the PI [48] and the Rubber Hand Illusion (RHI) [47] paradigms.

More precisely, we suggest that disinhibition of tactile neurons influences the Bayesian sensory inference process of body ownership in the RHI [82] by increasing the likelihood that spatial and temporal signals[4] have a single cause in the environment. We predict that such impairment weakens tactile discrimination and, as a consequence, increases the threshold at which visual and tactile stimulation are perceived as asynchronous. In turn, this rises the probability to experience the illusion of owning the rubber hand, in line with the Bayesian model mechanics [82].

[3] In this paradigm, two-point stimuli are administered by an aesthesiometer in the palm of the hand at different distances to detect the threshold at which an individual stops perceiving two separated stimuli.

[4] Bayesian modelling of the RHI [82] proposed that spatial signals are composed by visual and proprioceptive information of the hand location, whereas temporal signals are comprised by the synchronisation of visual and tactile stimulation

At the neurobiological level, our view is in line with reports of tactile discrimination being influenced by the inhibitory activity of GABA neurons. Specifically, magnetic resonance spectroscopy has consistently revealed that lower GABA concentration predicts higher discrimination thresholds (i.e. decreased accuracy in discrimination) in a tactile frequency discrimination task in healthy population [83], autism disorder [84, 85] and Tourette syndrome [86]. Plus, such lower concentration has also been found to be correlated with reports of tactile hypersensitivity [85]. Based on this evidence, we suggest that an impairment of GABA transmission is also behind the decreased two-point tactile discrimination found in the SCZ spectrum [79, 80, 81, 48] and the above described symptomatology.

4.4 Limitations

The presented modelling of the neural mechanism behind the observed PPS in SCZ and H-SPQ holds relevant limitations. One of them is that the network model [40] does not capture scaled RT differences when the sound is administered at different distance points[5]. Hence, the model accurately reproduces the shape of the PPS representation (i.e. central point and slope), but it is not able to reproduce realistic RT variability across distance points.

We overcame this by adding a linear regression model [73] to match the RT generated by the network to the scale observed in experimental data. By doing so we did not model sensorimotor mechanisms relevant to generate the behavioural response (i.e. button press) measured in the experimental task [4]. A further version of the model should include those mechanisms because the encoding of PPS is closely related to action generation [37, 36] and its impairment is related to deficits in the initiation and maintenance of activities (i.e. negative symptoms) in SCZ [4].

Another limitation is that the implementation of E/I balance modulation in the model is not biologically detailed. We implemented this modulation by including a bias term in the activation function of the unisensory neurons (see Section 2.4 for more details). In contrast to state of the art working memory models of SCZ [9, 10], our modelling does not directly manipulate NMDA synapses in inhibitory interneurons or excitatory neurons because the PPS network model was not built with such degree of biological detail [40].

[5]For example, the SCZ model registers differences of less than 1 ms, whereas differences of approximately 20 ms are observed in the experimental data.

Moreover, the network model employed for this study lacks realistic variability that can account for individual differences observed in the encoding of the PPS in healthy individuals [38, 40, 4]. This limitation would influence the results of the fitting procedure at the individual level, resulting in individual variability unrelated to the disease being attributed to β or ρ. Hence, a detailed analysis at the individual level and the exploration of potential correlations with symptoms and personality traits could be achieved only after improving this feature of the network model.

A further limitation is that hierarchical inference processes involved in perception were not modelled. This is particularly relevant because contemporary accounts of SCZ [12, 13, 14] consider that the main impairment of the disease is related to failures in such inference processes. Hence, the proposed effects of cortical disinhibition in PPS encoding, personal space delimitation and tactile discrimination should be further explored in terms of Bayesian inferences across different levels of the cortical hierarchy.

Finally, the experimental evidence directly assessing the PPS representation in SCZ is scarce. Our findings are based on the modelling of a single small study that employs one of the simplest experimental paradigms to behaviourally measure the PPS [4]. Thus, we encourage further studies with larger samples and more sophisticated behavioural [39] and neurocognitive measurements [87, 88, 89] of the PPS representation in the SCZ spectrum.

Chapter 5

Conclusions

We introduced a novel working model of PPS representation in SCZ compatible with current empirical evidence of self-aberrations, personal space, tactile discrimination and symptoms observed in patients. Computationally, we observed the influence of cortical disinhibition of sensory neurons in the PPS of SCZ patients and H-SPQ individuals. We also predicted that such disinhibition also influences the impairment in tactile discrimination and the enlargement of the personal space observed in patients. Based on these predictions, we proposed links between such behavioural observations and SCZ spectrum symptoms.

To our knowledge, this study is the first to approach PPS encoding in mental disorders computationally. Thus, this work contributes to computational psychiatry by opening the possibility to examine other diseases in which PPS is thought to be impaired, such as autism [90, 3], psychopathy [91], anxiety [92] and borderline personality disorders [93]. For this purpose, we encourage the development of models able to integrate the multisensory integration processes explored in this study within a predictive coding framework.

Bibliography

[1] B. Nelson, A. Fornito, B. Harrison, M. Yücel, L. Sass, A. Yung, A. Thompson, S. Wood, C. Pantelis, and P. McGorry, "A disturbed sense of self in the psychosis prodrome: linking phenomenology and neurobiology," *Neuroscience & Biobehavioral Reviews*, vol. 33, no. 6, pp. 807–817, 2009.

[2] B. Nelson and L. A. Sass, "Towards integrating phenomenology and neurocognition: Possible neurocognitive correlates of basic self-disturbance in schizophrenia," *Current Problems of Psychiatry*, vol. 18, no. 3, pp. 184–200, 2017.

[3] J.-P. Noel, C. J. Cascio, M. T. Wallace, and S. Park, "The spatial self in schizophrenia and autism spectrum disorder," *Schizophrenia research*, vol. 179, pp. 8–12, 2017.

[4] G. Di Cosmo, M. Costantini, A. Salone, G. Martinotti, G. Di Iorio, M. Di Giannantonio, and F. Ferri, "Peripersonal space boundary in schizotypy and schizophrenia," *Schizophrenia research*, 2017.

[5] R. E. Hoffman and S. K. Dobscha, "Cortical pruning and the development of schizophrenia: a computer model," *Schizophrenia bulletin*, vol. 15, no. 3, pp. 477–490, 1989.

[6] R. E. Hoffman, J. Rapaport, R. Ameli, T. H. McGlashan, D. Harcherik, and D. Servan-Schreiber, "A neural network simulation of hallucinated voices and associated speech perception impairments in schizophrenic patients," *Journal of Cognitive Neuroscience*, vol. 7, no. 4, pp. 479–496, 1995.

[7] I. Feinberg, "Efference copy and corollary discharge: implications for thinking and its disorders.," *Schizophrenia bulletin*, vol. 4, no. 4, p. 636, 1978.

[8] D. M. Wolpert, Z. Ghahramani, and M. I. Jordan, "An internal model for sensorimotor integration," *Science*, vol. 269, no. 5232, pp. 1880–1882, 1995.

[9] E. T. Rolls and G. Deco, "A computational neuroscience approach to schizophrenia and its onset," *Neuroscience & Biobehavioral Reviews*, vol. 35, no. 8, pp. 1644–1653, 2011.

[10] J. D. Murray, A. Anticevic, M. Gancsos, M. Ichinose, P. R. Corlett, J. H. Krystal, and X.-J. Wang, "Linking microcircuit dysfunction to cognitive impairment: effects of disinhibition associated with schizophrenia in a cortical working memory model," *Cerebral cortex*, vol. 24, no. 4, pp. 859–872, 2012.

[11] R. Jardri, K. Hugdahl, M. Hughes, J. Brunelin, F. Waters, B. Alderson-Day, D. Smailes, P. Sterzer, P. R. Corlett, P. Leptourgos, *et al.*, "Are hallucinations due to an imbalance between excitatory and inhibitory influences on the brain?," *Schizophrenia bulletin*, vol. 42, no. 5, pp. 1124–1134, 2016.

[12] R. A. Adams, K. E. Stephan, H. R. Brown, C. D. Frith, and K. J. Friston, "The computational anatomy of psychosis," *Frontiers in psychiatry*, vol. 4, p. 47, 2013.

[13] K. Friston, H. R. Brown, J. Siemerkus, and K. E. Stephan, "The dysconnection hypothesis (2016)," *Schizophrenia research*, vol. 176, no. 2-3, pp. 83–94, 2016.

[14] P. Sterzer, R. A. Adams, P. Fletcher, C. Frith, S. M. Lawrie, L. Muckli, P. Petrovic, P. Uhlhaas, M. Voss, and P. R. Corlett, "The predictive coding account of psychosis," *Biological psychiatry*, vol. 84, no. 9, pp. 634–643, 2018.

[15] A. Clark, *Surfing uncertainty: Prediction, action, and the embodied mind*. Oxford University Press, 2015.

[16] A. M. Bastos, W. M. Usrey, R. A. Adams, G. R. Mangun, P. Fries, and K. J. Friston, "Canonical microcircuits for predictive coding," *Neuron*, vol. 76, no. 4, pp. 695–711, 2012.

[17] S. Shipp, "Neural elements for predictive coding," *Frontiers in psychology*, vol. 7, p. 1792, 2016.

[18] P. R. Corlett, G. D. Honey, J. H. Krystal, and P. C. Fletcher, "Glutamatergic model psychoses: prediction error, learning, and inference," *Neuropsychopharmacology*, vol. 36, no. 1, p. 294, 2011.

[19] C.-E. Notredame, D. Pins, S. Deneve, and R. Jardri, "What visual illusions teach us about schizophrenia," *Frontiers in integrative neuroscience*, vol. 8, p. 63, 2014.

[20] A. R. Powers, C. Mathys, and P. Corlett, "Pavlovian conditioning–induced hallucinations result from overweighting of perceptual priors," *Science*, vol. 357, no. 6351, pp. 596–600, 2017.

[21] C. M. Cassidy, P. D. Balsam, J. J. Weinstein, R. J. Rosengard, M. Slifstein, N. D. Daw, A. Abi-Dargham, and G. Horga, "A perceptual inference mechanism for hallucinations linked to striatal dopamine," *Current Biology*, vol. 28, no. 4, pp. 503–514, 2018.

[22] D. Benrimoh, T. Parr, P. Vincent, R. A. Adams, and K. Friston, "Active inference and auditory hallucinations," *Computational Psychiatry*, vol. 2, pp. 183–204, 2018.

[23] H. Brown, R. A. Adams, I. Parees, M. Edwards, and K. Friston, "Active inference, sensory attenuation and illusions," *Cognitive processing*, vol. 14, no. 4, pp. 411–427, 2013.

[24] P. Sterzer, A. L. Mishara, M. Voss, and A. Heinz, "Thought insertion as a self-disturbance: an integration of predictive coding and phenomenological approaches," *Frontiers in human neuroscience*, vol. 10, p. 502, 2016.

[25] P. J. Harrison, "The neuropathology of schizophrenia: a critical review of the data and their interpretation," *Brain*, vol. 122, no. 4, pp. 593–624, 1999.

[26] I. Ellison-Wright and E. Bullmore, "Meta-analysis of diffusion tensor imaging studies in schizophrenia," *Schizophrenia research*, vol. 108, no. 1-3, pp. 3–10, 2009.

[27] N. van der Stoep, T. Nijboer, and A. Postma, "Multisensory perception and the coding of space," *Neuropsychology of Space: Spatial Functions of the Human Brain*, vol. 123, 2016.

[28] L. Fogassi, V. Gallese, L. Fadiga, G. Luppino, M. Matelli, and G. Rizzolatti, "Coding of peripersonal space in inferior premotor cortex (area f4)," *Journal of neurophysiology*, vol. 76, no. 1, pp. 141–157, 1996.

[29] M. S. Graziano, L. A. Reiss, and C. G. Gross, "A neuronal representation of the location of nearby sounds," *Nature*, vol. 397, no. 6718, p. 428, 1999.

[30] G. di Pellegrino, E. Ladavas, and A. Farné, "Seeing where your hands are," *Nature*, vol. 388, no. 6644, p. 730, 1997.

[31] E. Làdavas, G. d. Pellegrino, A. Farnè, and G. Zeloni, "Neuropsychological evidence of an integrated visuotactile representation of peripersonal space in humans," *Journal of Cognitive Neuroscience*, vol. 10, no. 5, pp. 581–589, 1998.

[32] G. Gentile, A. Guterstam, C. Brozzoli, and H. H. Ehrsson, "Disintegration of multisensory signals from the real hand reduces default limb self-attribution: an fmri study," *Journal of Neuroscience*, vol. 33, no. 33, pp. 13350–13366, 2013.

[33] C. Brozzoli, H. H. Ehrsson, and A. Farnè, "Multisensory representation of the space near the hand: from perception to action and interindividual interactions," *The Neuroscientist*, vol. 20, no. 2, pp. 122–135, 2014.

[34] F. Bernasconi, J.-P. Noel, H. D. Park, N. Faivre, M. Seeck, L. Spinelli, K. Schaller, O. Blanke, and A. Serino, "Audio-tactile and peripersonal space processing around the trunk in human parietal and temporal cortex: an intracranial eeg study," *Cerebral Cortex*, vol. 28, no. 9, pp. 3385–3397, 2018.

[35] J.-P. Noel, A. Serino, and M. T. Wallace, "Increased neural strength and reliability to audiovisual stimuli at the boundary of peripersonal space," *Journal of cognitive neuroscience*, pp. 1–18, 2018.

[36] P. Grivaz, O. Blanke, and A. Serino, "Common and distinct brain regions processing multisensory bodily signals for peripersonal space and body ownership," *Neuroimage*, vol. 147, pp. 602–618, 2017.

[37] M. S. Graziano and D. F. Cooke, "Parieto-frontal interactions, personal space, and defensive behavior," *Neuropsychologia*, vol. 44, no. 6, pp. 845–859, 2006.

[38] E. Canzoneri, E. Magosso, and A. Serino, "Dynamic sounds capture the boundaries of peripersonal space representation in humans," *PloS one*, vol. 7, no. 9, p. e44306, 2012.

[39] A. Serino, J.-P. Noel, G. Galli, E. Canzoneri, P. Marmaroli, H. Lissek, and O. Blanke, "Body part-centered and full body-centered peripersonal space representations," *Scientific reports*, vol. 5, p. 18603, 2015.

[40] A. Serino, E. Canzoneri, M. Marzolla, G. Di Pellegrino, and E. Magosso, "Extending peripersonal space representation without tool-use: evidence from a combined behavioral-computational approach," *Frontiers in behavioral neuroscience*, vol. 9, p. 4, 2015.

[41] O. Blanke, M. Slater, and A. Serino, "Behavioral, neural, and computational principles of bodily self-consciousness," *Neuron*, vol. 88, no. 1, pp. 145–166, 2015.

[42] J.-P. Noel, O. Blanke, and A. Serino, "From multisensory integration in peripersonal space to bodily self-consciousness: from statistical regularities to statistical inference," *Annals of the New York Academy of Sciences*, vol. 1426, no. 1, pp. 146–165, 2018.

[43] J.-P. Noel, M. Samad, A. Doxon, J. Clark, S. Keller, and M. Di Luca, "Peripersonal space as a prior in coupling visual and proprioceptive signals," *Scientific reports*, vol. 8, no. 1, p. 15819, 2018.

[44] A. Serino, "Peripersonal space (pps) as a multisensory interface between the individual and the environment, defining the space of the self," *Neuroscience & Biobehavioral Reviews*, 2019.

[45] E. Magosso, M. Zavaglia, A. Serino, G. Di Pellegrino, and M. Ursino, "Visuotactile representation of peripersonal space: a neural network study," *Neural computation*, vol. 22, no. 1, pp. 190–243, 2010.

[46] J.-P. Noel, O. Blanke, E. Magosso, and A. Serino, "Neural adaptation accounts for the dynamic resizing of peri-personal space: evidence from a psychophysical-computational approach," *Journal of neurophysiology*, 2018.

[47] K. N. Thakkar, H. S. Nichols, L. G. McIntosh, and S. Park, "Disturbances in body ownership in schizophrenia: evidence from the rubber hand illusion and case study of a spontaneous out-of-body experience," *PloS one*, vol. 6, no. 10, p. e27089, 2011.

[48] J. Michael and S. Park, "Anomalous bodily experiences and perceived social isolation in schizophrenia: An extension of the social deafferentation hypothesis," *Schizophrenia research*, vol. 176, no. 2-3, pp. 392–397, 2016.

[49] O. Mason and G. Claridge, "The oxford-liverpool inventory of feelings and experiences (o-life): further description and extended norms," *Schizophrenia research*, vol. 82, no. 2-3, pp. 203–211, 2006.

[50] J.-P. Noel, H.-D. Park, I. Pasqualini, H. Lissek, M. Wallace, O. Blanke, and A. Serino, "Audio-visual sensory deprivation degrades visuo-tactile peri-personal space," *Consciousness and cognition*, vol. 61, pp. 61–75, 2018.

[51] A. Pelletier-Baldelli and D. J. Holt, "Shared neural substrates of deficits in social cognition and negative symptoms in schizophrenia," in *Social Cognition in Psychosis*, pp. 125–142, Elsevier, 2019.

[52] M. J. Horowitz, D. F. Duff, and L. O. Stratton, "Body-buffer zone: exploration of personal space," *Archives of general psychiatry*, vol. 11, no. 6, pp. 651–656, 1964.

[53] M. P. Duke and C. Mullens, "Preferred interpersonal distance as a function of locus of control orientation in chronic schizophrenics, nonschizophrenic patients, and normals.," *Journal of Consulting and Clinical Psychology*, vol. 41, no. 2, p. 230, 1973.

[54] P. Srivastava and M. K. Mandal, "Proximal spacing to facial affect expressions in schizophrenia," *Comprehensive psychiatry*, vol. 31, no. 2, pp. 119–124, 1990.

[55] Y. Nechamkin, I. Salganik, I. Modai, and A. M. Ponizovsky, "Interpersonal distance in schizophrenic patients: relationship to negative syndrome," *International Journal of Social Psychiatry*, vol. 49, no. 3, pp. 166–174, 2003.

[56] V. Deuš and N. Jokić-Begić, "Personal space in schizophrenic patients," *Psychiatria Danubina*, vol. 18, no. 3-4, p. 150, 2006.

[57] S.-H. Park, J. Ku, J.-J. Kim, H. J. Jang, S. Y. Kim, S. H. Kim, C.-H. Kim, H. Lee, I. Y. Kim, and S. I. Kim, "Increased personal space of patients with schizophrenia in a virtual social environment," *Psychiatry research*, vol. 169, no. 3, pp. 197–202, 2009.

[58] D. J. Holt, E. A. Boeke, G. Coombs III, S. N. DeCross, B. S. Cassidy, S. Stufflebeam, S. L. Rauch, and R. B. Tootell, "Abnormalities in personal space and parietal–frontal function in schizophrenia," *NeuroImage: Clinical*, vol. 9, pp. 233–243, 2015.

[59] D. J. Holt, B. S. Cassidy, X. Yue, S. L. Rauch, E. A. Boeke, S. Nasr, R. B. Tootell, and G. Coombs, "Neural correlates of personal space intrusion," *Journal of Neuroscience*, vol. 34, no. 12, pp. 4123–4134, 2014.

[60] J. B. Vieira, S. R. Pierzchajlo, and D. G. Mitchell, "Neural correlates of social and non-social personal space intrusions: role of defensive and peripersonal space systems in interpersonal distance regulation," *Social neuroscience*, no. just-accepted, 2019.

[61] E. Magosso, M. Ursino, G. di Pellegrino, E. Làdavas, and A. Serino, "Neural bases of peri-hand space plasticity through tool-use: insights from a combined computational–experimental approach," *Neuropsychologia*, vol. 48, no. 3, pp. 812–830, 2010.

[62] C. Cavada and P. S. Goldman-Rakic, "Posterior parietal cortex in rhesus monkey: Ii. evidence for segregated corticocortical networks linking sensory and limbic areas with the frontal lobe," *Journal of Comparative Neurology*, vol. 287, no. 4, pp. 422–445, 1989.

[63] J. W. Lewis and D. C. Van Essen, "Corticocortical connections of visual, sensorimotor, and multimodal processing areas in the parietal lobe of the macaque monkey," *Journal of Comparative Neurology*, vol. 428, no. 1, pp. 112–137, 2000.

[64] G. Rizzolatti, C. Scandolara, M. Matelli, and M. Gentilucci, "Afferent properties of periarcuate neurons in macaque monkeys. ii. visual responses," *Behavioural brain research*, vol. 2, no. 2, pp. 147–163, 1981.

[65] M. S. Graziano, X. T. Hu, and C. G. Gross, "Visuospatial properties of ventral premotor cortex," *Journal of neurophysiology*, vol. 77, no. 5, pp. 2268–2292, 1997.

[66] A. Iriki, M. Tanaka, S. Obayashi, and Y. Iwamura, "Self-images in the video monitor coded by monkey intraparietal neurons," *Neuroscience research*, vol. 40, no. 2, pp. 163–173, 2001.

[67] A. Maravita and A. Iriki, "Tools for the body (schema)," *Trends in cognitive sciences*, vol. 8, no. 2, pp. 79–86, 2004.

[68] A. Schlack, S. J. Sterbing-D'Angelo, K. Hartung, K.-P. Hoffmann, and F. Bremmer, "Multisensory space representations in the macaque ventral intraparietal area," *Journal of Neuroscience*, vol. 25, no. 18, pp. 4616–4625, 2005.

[69] P. Dayan, L. F. Abbott, and L. Abbott, "Theoretical neuroscience: computational and mathematical modeling of neural systems," 2001.

[70] R. Hoffman and T. McGlashan, "Using a speech perception neural network computer simulation to contrast neuroanatomic versus neuromodulatory models of auditory hallucinations," *Pharmacopsychiatry*, vol. 39, no. S 1, pp. 54–64, 2006.

[71] G. M. Edelman, "Neural darwinism: selection and reentrant signaling in higher brain function," *Neuron*, vol. 10, no. 2, pp. 115–125, 1993.

[72] P. G. Nelson, R. D. Fields, C. Yu, and E. A. Neale, "Mechanisms involved in activity-dependent synapse formation in mammalian central nervous system cell cultures," *Journal of neurobiology*, vol. 21, no. 1, pp. 138–156, 1990.

[73] R. Bogacz and J. D. Cohen, "Parameterization of connectionist models," *Behavior Research Methods, Instruments, & Computers*, vol. 36, no. 4, pp. 732–741, 2004.

[74] R. Storn and K. Price, "Differential evolution–a simple and efficient heuristic for global optimization over continuous spaces," *Journal of global optimization*, vol. 11, no. 4, pp. 341–359, 1997.

[75] Y. Delevoye-Turrell, C. Vienne, and Y. Coello, "Space boundaries in schizophrenia," *Social Psychology*, 2011.

[76] C. Teneggi, E. Canzoneri, G. di Pellegrino, and A. Serino, "Social modulation of peripersonal space boundaries," *Current biology*, vol. 23, no. 5, pp. 406–411, 2013.

[77] T. C. Ford, R. Nibbs, and D. P. Crewther, "Increased glutamate/gaba+ ratio in a shared autistic and schizotypal trait phenotype termed social disorganisation," *NeuroImage: Clinical*, vol. 16, pp. 125–131, 2017.

[78] T. C. Ford, R. Nibbs, and D. P. Crewther, "Glutamate/gaba+ ratio is associated with the psychosocial domain of autistic and schizotypal traits," *PloS one*, vol. 12, no. 7, p. e0181961, 2017.

[79] M. F. Lenzenweger, "Two-point discrimination thresholds and schizotypy: illuminating a somatosensory dysfunction," *Schizophrenia research*, vol. 42, no. 2, pp. 111–124, 2000.

[80] B. P. Chang and M. F. Lenzenweger, "Somatosensory processing in the biological relatives of schizophrenia patients: A signal detection analysis of two-point discrimination.," *Journal of abnormal psychology*, vol. 110, no. 3, p. 433, 2001.

[81] B. P. Chang and M. F. Lenzenweger, "Somatosensory processing and schizophrenia liability: proprioception, exteroceptive sensitivity, and graphesthesia performance in the biological relatives of schizophrenia patients.," *Journal of abnormal psychology*, vol. 114, no. 1, p. 85, 2005.

[82] M. Samad, A. J. Chung, and L. Shams, "Perception of body ownership is driven by bayesian sensory inference," *PloS one*, vol. 10, no. 2, p. e0117178, 2015.

[83] N. A. Puts, R. A. Edden, C. J. Evans, F. McGlone, and D. J. McGonigle, "Regionally specific human gaba concentration correlates with tactile discrimination thresholds," *Journal of Neuroscience*, vol. 31, no. 46, pp. 16556–16560, 2011.

[84] N. A. Puts, A. D. Harris, D. Crocetti, C. Nettles, H. S. Singer, M. Tommerdahl, R. A. Edden, and S. H. Mostofsky, "Reduced gabaergic inhibition and abnormal sensory symptoms in children with tourette syndrome," *Journal of neurophysiology*, vol. 114, no. 2, pp. 808–817, 2015.

[85] L.-A. Sapey-Triomphe, F. Lamberton, S. Sonié, J. Mattout, and C. Schmitz, "Tactile hypersensitivity and gaba concentration in the sensorimotor cortex of adults with autism," *Autism Research*, vol. 12, no. 4, pp. 562–575, 2019.

[86] N. A. Puts, E. L. Wodka, A. D. Harris, D. Crocetti, M. Tommerdahl, S. H. Mostofsky, and R. A. Edden, "Reduced gaba and altered somatosensory function in children with autism spectrum disorder," *Autism Research*, vol. 10, no. 4, pp. 608–619, 2017.

[87] A. Naro, R. S. Calabrò, G. La Rosa, V. A. Andronaco, L. Billeri, P. Lauria, A. Bramanti, and P. Bramanti, "Toward understanding the neurophysiological basis of peripersonal space: An eeg study on healthy individuals," *PloS one*, vol. 14, no. 6, p. e0218675, 2019.

[88] J.-P. Noel, A. Serino, and M. T. Wallace, "Increased neural strength and reliability to audiovisual stimuli at the boundary of peripersonal space," *Journal of cognitive neuroscience*, vol. 31, no. 8, pp. 1155–1172, 2019.

[89] J.-P. Noel, C. Chatelle, S. Perdikis, J. Jöhr, M. L. Da Silva, P. Ryvlin, M. De Lucia, J. d. R. Millán, K. Diserens, and A. Serino, "Peri-personal space encoding in patients with disorders of consciousness and cognitive-motor dissociation," *NeuroImage: Clinical*, p. 101940, 2019.

[90] C. J. Cascio, J. H. Foss-Feig, C. P. Burnette, J. L. Heacock, and A. A. Cosby, "The rubber hand illusion in children with autism spectrum disorders: delayed influence of combined tactile and visual input on proprioception," *Autism*, vol. 16, no. 4, pp. 406–419, 2012.

[91] R. Welsch, H. Hecht, and C. von Castell, "Psychopathy and the regulation of interpersonal distance," *Clinical Psychological Science*, vol. 6, no. 6, pp. 835–847, 2018.

[92] M. Taffou and I. Viaud-Delmon, "Cynophobic fear adaptively extends peripersonal space," *Frontiers in psychiatry*, vol. 5, p. 122, 2014.

[93] A. Schienle, A. Wabnegger, F. Schöngassner, and V. Leutgeb, "Effects of personal space intrusion in affective contexts: an fmri investigation with women suffering from borderline personality disorder," *Social cognitive and affective neuroscience*, vol. 10, no. 10, pp. 1424–1428, 2015.

Appendix A

Network model implementation

A.1 Values of HC model parameters

Unisensory receptive fields			
$\phi_0^t = 1$	$\sigma_\phi^t = 1$	$\phi_0^a = 1$	$\sigma_\phi^a = 10$
External stimuli			
$I_0^t = 2.5$	$\sigma_I^t = 0.3$ cm	$I_0^a = 3.6$	$\sigma_I^a = 0.3$ cm
Lateral synapses in unisensory areas			
$L_{ex}^t = 0.15$	$L_{in}^t = 0.05$	$\sigma_{ex}^t = 1$ cm	$\sigma_{in}^t = 1$ cm
$L_{ex}^a = 0.15$	$L_{in}^a = 0.05$	$\sigma_{ex}^a = 20$ cm	$\sigma_{in}^a = 80$ cm
Feedforward and feedback synapses			
$W_0^t = 6.5$	$W_0^a = 6.5$	$B_0^t = 2.5$	$B_0^a = 2.5$
$k_1 = 15.42$ cm	$k_2 = 813.75$ cm	$\alpha = 0.9$	Lim = 66.09 cm
Input-output relationship of unisensory neurons			
f_{mim}^t = -0.12	$f_{max}^t = 1$	$q_c^t = 19.43$	$r^t = 0.34$
f_{mim}^a = -0.12	$f_{max}^a = 1$	$q_c^a = 19.43$	$r^a = 0.34$
$\tau = 20$ ms			
Input-output relationship of the multisensory neuron			
$f_{mim}^m = 0$	$f_{max}^m = 1$	$q_c^m = 12$	$r^m = 0.6$
$\tau = 20$ ms			

Table A.1: Values of the parameters in the HC model. This parameterisation remained fixed throughout the simulations computed to identify the SCZ and H-SPQ models.

A.2 Unisensory neurons input

The unisensory neurons input $u_{ij}^{s}(t)$ is computed by Equation A.1.

$$u_{ij}^{s}(t) = \varphi_{ij}^{s} + I_{ij}^{s}(t) + b_{ij}^{s}(t), \qquad s = t, a \tag{A.1}$$

The term φ_{ij}^{s} denotes the input due to external stimulus, $I_{ij}^{s}(t)$ indicates the input received from other neurons in the same area and $b_{ij}^{s}(t)$ represents the feedback input from the multisensory neuron.

The input φ_{ij}^{s} is defined by Equation A.2.

$$\varphi_{ij}^{s} = \sum_{l}\sum_{n} \Phi_{ij}^{s}(x_l, y_n) \cdot I^{s}(x_l, y_n)\, \Delta x_l \Delta y_n, \qquad s = t, a \tag{A.2}$$

The expression $I^{s}(x_l, y_n)$ denotes the external stimulus applied at coordinates x and y, as defined in Equation 2.12. The term $\Phi_{ij}^{s}(x_l, y_n)$ represents the RF of the unisensory neuron *ij* in the unisensory area *s*. Equation A.2 is solved by considering $\Delta x_l = \Delta y_n = 0.2cm$.

The RF $\Phi_{ij}^{s}(x_l, y_n)$ is defined by the Gaussian function presented in Equation A.3.

$$\Phi_{ij}^{s}(x,y) = \Phi_{0}^{s} \cdot exp\left(-\frac{(x_i^s - x)^2 + \left(y_j^s - y\right)^2}{2 \cdot \left(\sigma_{\Phi}^{s}\right)^2} \right), \qquad s = t, a \tag{A.3}$$

The terms x_i and y_j denote the coordinates of the RF centre, whereas x and y represent spatial coordinates within the unisensory areas. The parameters Φ_0^s and σ_{Φ}^{s} govern the amplitude and standard deviation of the Gaussian function that define the RF of the unisensory neurons.

Following with Equation A.1 description, the lateral inputs $I_{ij}^{s}(t)$ were calculated by Equation A.4.

$$I_{ij}^{s} = \sum_{h=1}^{N^s}\sum_{k=1}^{M^s} L_{ij,hk}^{s} \cdot z_{hk}^{s}(t), \qquad s = t, a \tag{A.4}$$

The term $L_{ij,hk}^{s}$ indicates the synaptic weights calculated by Equation 2.3 and displayed in Figure 2.4. Similarly, $z_{hk}^{s}(t)$ denotes the neuron activation at time *t*, as described by equation 2.9.

Finally, the feedback input $b_{ij}^{s}(t)$ was computed by Equation A.5.

$$b_{ij}^{s}(t) = B_{ij}^{s} \cdot z^{m}(t), \qquad s = t, a \tag{A.5}$$

The term B_{ij}^{s} represents the strenght of feedback synapses, as described by equation 2.7. The expression $z^{m}(t)$ denotes the activation state of the multisensory neuron at time t (more details in Appendix A.3).

A.3 Multisensory neuron activity

The activity of the multisensory neuron is computed by the following equations:

$$\tau \frac{dq^{m}(t)}{dt} = -q^{m}(t) + u^{m}(t) \tag{A.6}$$

$$z^{m}(t) = \Psi(q^{m}(t)) \cdot H(\Psi(q^{m}(t))) \tag{A.7}$$

$$\Psi(q^{m}(t)) = \frac{f_{min}^{m} + f_{max}^{m} \cdot e^{(q^{m} - q_{c}) \cdot r^{m}}}{1 + e^{(q^{m} - q_{c}) \cdot r^{m}}} \tag{A.8}$$

The term $u^{m}(t)$ represents the multisensory neuron input described by Equation 2.11. The description of the remaining terms are analogous to Equations 2.8,2.9 and 2.10.

A.4 Sigmoidal fit of model outputs

The RT values generated by the network in the experiment simulation were fitted to a sigmoid function described by Equation A.9.

$$f_{RT}(D) = \frac{\eta_{min} + \eta_{max} \cdot e^{\frac{(D - D_{c})}{h}}}{1 + e^{\frac{(D - D_{c})}{h}}} \tag{A.9}$$

The term D denotes the distance from the hand in cm at which the auditory stimulus was applied. The parameters η_{min} and η_{max} represent the lower and upper saturation of the sigmoidal relationship. D_{c} is the central point of the function and h denotes the slope of the function at its central point.

All the four parameters of the function were estimated by a least-squares fitting procedure. The estimated value of the sigmoid central point D_{c} was assumed as the

boundary of the PPS representation generated by the model and the value of the slope h the sharpness of its definition.

Appendix B

Modelling of SCZ and SPQ in the network

B.1 Pruning threshold exploration

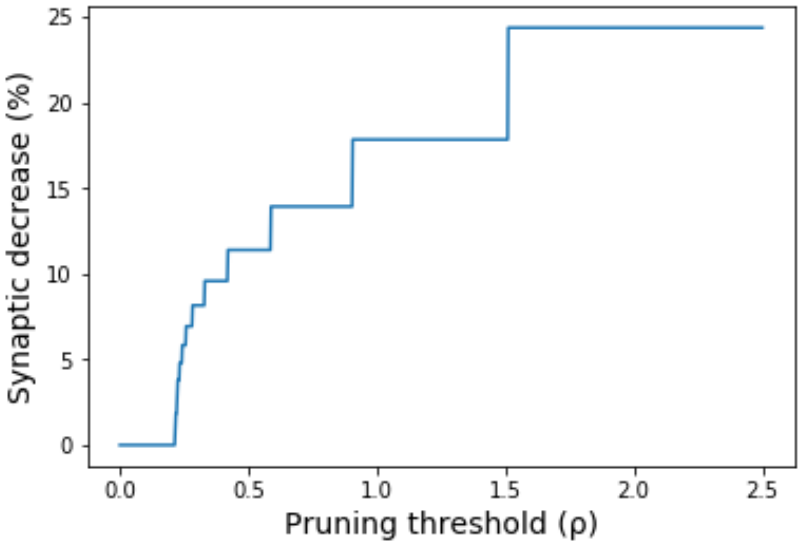

Figure B.1: Pruning threshold influence in synaptic density decrease. The plot illustrates how the synaptic decrease increases as the pruning threshold increases. The results reveal the presence of flat regions in the plotted function.

Appendix C

Results

C.1 PPS representation under E/I modulation

The influence of disinhibition in the PPS representation computed by the network model is presented in Figure C.1. The top panel indicates that the slope of the PPS remains almost constant as the unisensory areas get more desinhibited. In contrast, the bottom panel reveals that disinhibition of unisensory areas decreases the size of the PPS.

Analogously, the influence of reduced excitability in the PPS representation computed by the network model is presented in Figure C.2. Results presented in the top panel indicate that excitability reduction in unisensory areas sharpens the slope of the PPS. Conversely, the bottom panel shows that excitability reduction modulates the size of the PPS but less than in inhibition reduction.

Overall, the simulations presented in this section reveal that the modulation of the E/I balance in the unisensory areas is relevant to influence the size of the PPS representation. More precisely, it was observed that both inhibition and excitability reduction are capable of reducing the size of the PPS, whereas only excitability reduction sharpens the slope of the PPS.

C.2 PPS representation under decreased synaptic density

The influence of evolutionary pruning of top-down and bottom-up synapses in the PPS representation computed by the network is presented in Figure C.3. The top panel

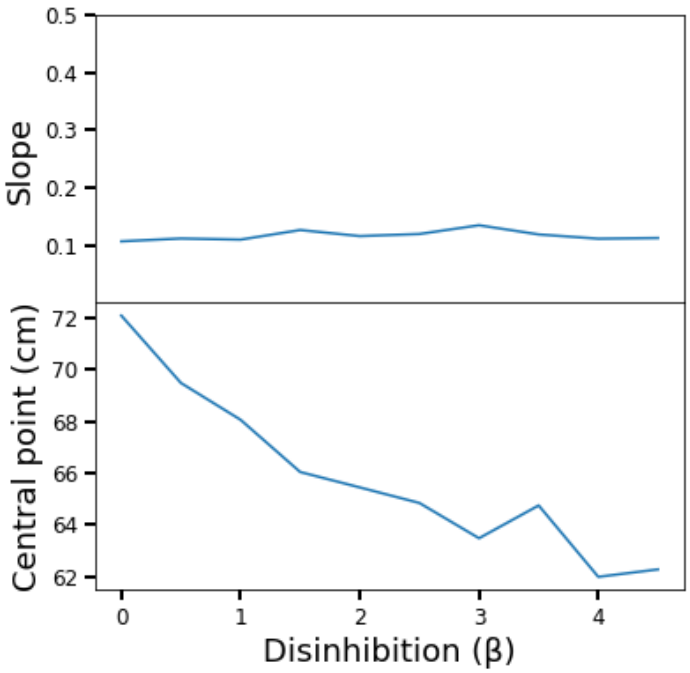

Figure C.1: Effect of inhibition reduction in PPS representation. Blue lines depict the features (slope and central point) of the PPS representation generated by the model at different levels of disinhibition.

shows that the slope loosens at low levels of synaptic pruning and sharpens as the level of synaptic pruning increases. In addition, the bottom panel indicates that the PPS computed by the network expands at low levels of synaptic pruning and narrows as the pruning level increases.

The simulations presented throughout this section reveal that the decrease of synaptic density in feedforward and feedback connections is relevant to reproduce the PPS representation of SCZ patients and H-SPQ individuals. More precisely, it was observed that the pruning level was able to modulate both the size and the slope of the PPS representation generated by the network.

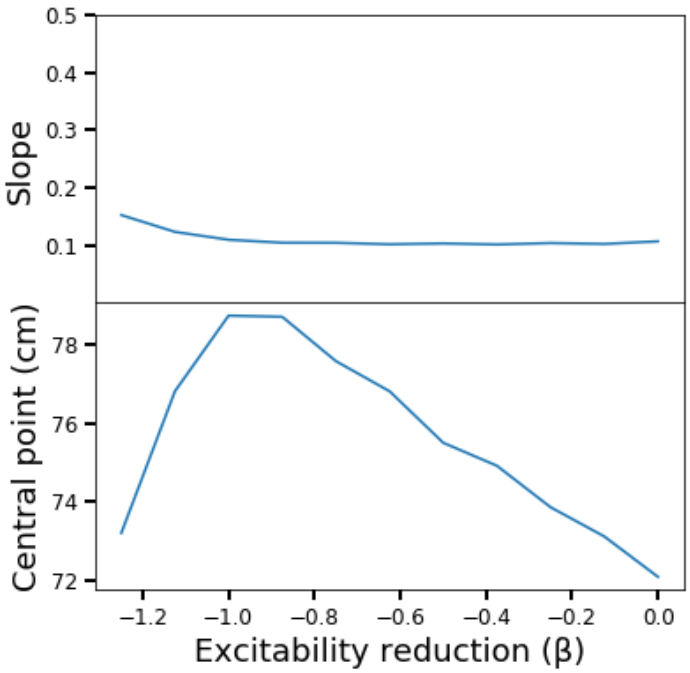

Figure C.2: Effect of excitability reduction in PPS representation. Blue lines illustrate the features of the PPS representation generated by the model at different levels of excitation reduction.

C.3 PPS representation under E/I modulation and decreased synaptic density

The combined effect of excitability reduction and decreased synaptic density on PPS representation is displayed in Figure C.4. Results shown in the top panel overall indicate that slopes are more steeped as the pruning level increases and that excitability reduction increases the effects of pruning on the steepness of the PPS representation. Similarly, the bottom panel indicates that the size of the PPS decreases as the pruning gets more intensive and that excitability reduction increases the effect of pruning on the size of the PPS

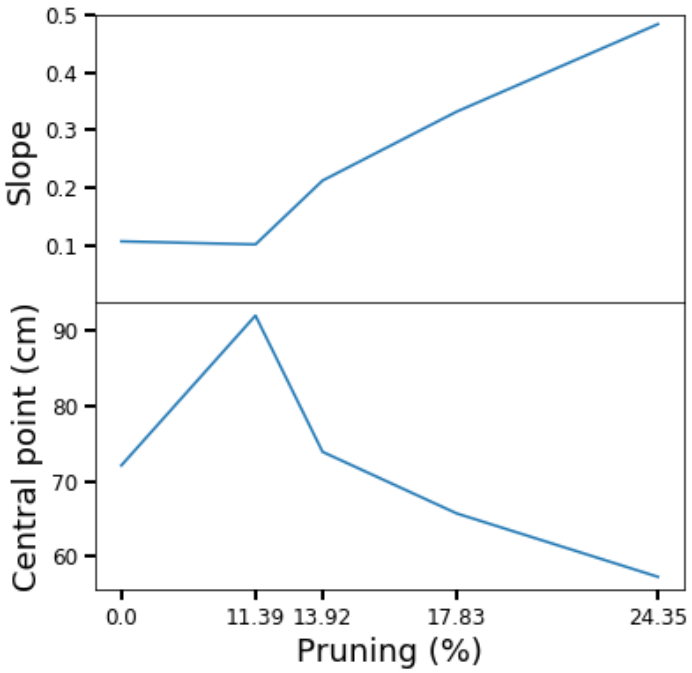

Figure C.3: Effect of decreased synaptic density in PPS representation. Blue lines illustrate the features of the PPS representation generated by the model at different levels of pruning.

C.4 Mechanics of the model in the simulated experiment

C.4.1 Mechanics of the H-SPQ model

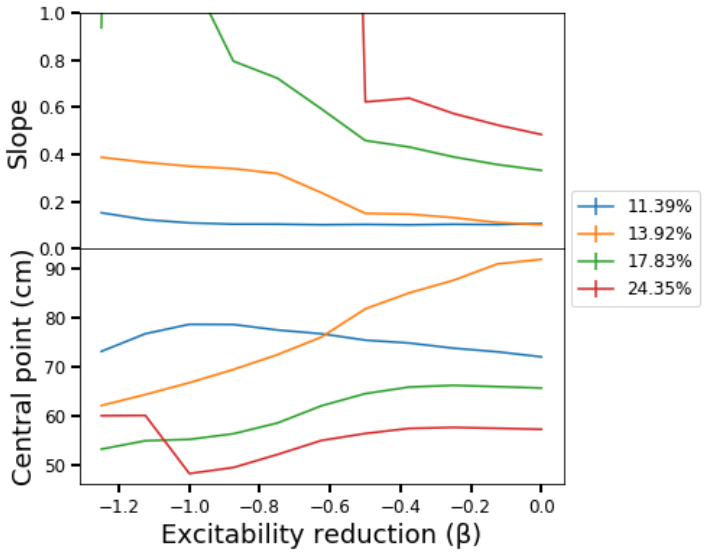

Figure C.4: Effect of excitability reduction and decreased synaptic density in PPS representation. Excitability reduction modulates the effects of pruning by increasing the steepness and reducing the size of the PPS representation.

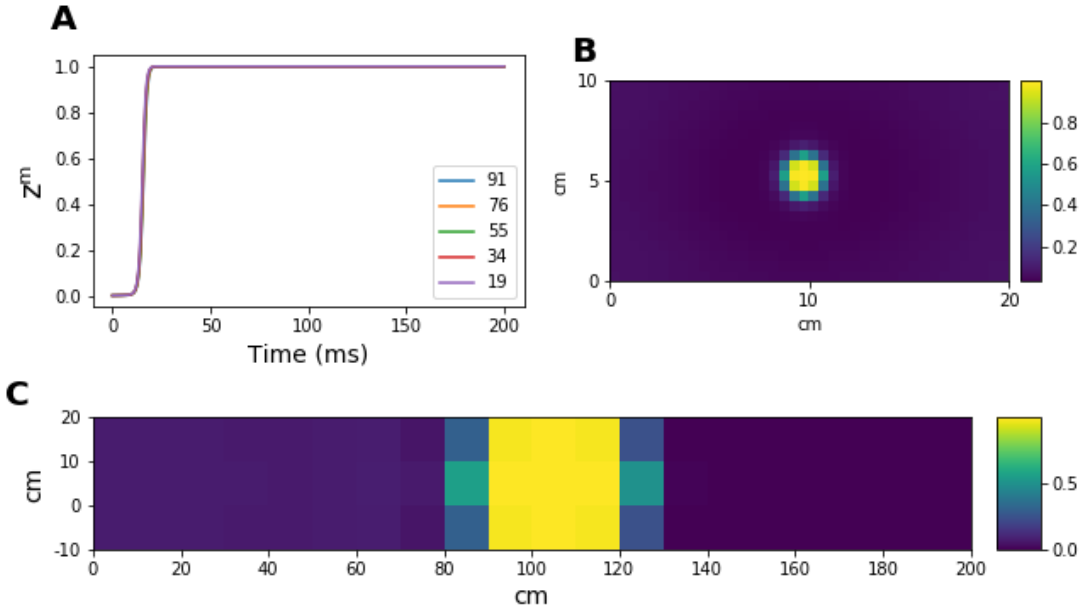

Figure C.5: H-SPQ network mechanics under audio-tactile stimulation. Description of **Figures A, B and C** are the same as those in Figure 3.3. The images illustrate that the multisensory neuron activity does not change across distances and that unisensory neurons activity spreads beyond the coordinates at which the stimuli were delivered.